USGS External Grant: G11AP20046

Strong Ground Motions in Salt Lake City and Other Metropolitan Areas from Large Earthquakes on the Wasatch Fault

Earth Research Institute
University of California, Santa Barbara

Ralph J. Archuleta
Department of Earth Science and Earth Research Institute
(805) 893-8441
Fax: (805) 893-2314
01/01/2011 through 12/31/2011 with no-cost extension through 12/31/2012

Abstract

We simulate M_W ~7.0 earthquakes on the Salt Lake City Segment of the Wasatch Fault to compute the ground motion that will affect the built environment in the Salt Lake City area. Using a finite element code we simulate the earthquakes as spontaneously propagating ruptures on a 50˚–dipping fault that is embedded in a 3D velocity structure. The initial stress conditions, a friction law (slip weakening), 3D structure that has both velocity strengthening and velocity weakening regions, various hypocenter locations and the geometry of the fault determine the dynamics of the rupture and consequently the ground motion. We considered many different cases that take into account variability of the initial stress, segmentation of the Wasatch Fault, and a geometry that accounts for the variations of the strike of the fault.

Contents

1 Introduction and Overview **4**

2 Model set-up **5**
2.1 Plan view of the study area 5
2.2 Finite element code 6
2.2.1 Fault plane construction 6
2.2.2 Mesh generation 6
2.2.3 Incorporating WFCVM3.0 7
2.2.4 Main parameters set-up 7

3 Modeling single fault **8**
3.1 Tests of healing parameters 8
3.2 Tests of shallow layer stress tapering (one way to reduce surface calculated offset) 9
3.3 Tests of shallow layer velocity strengthening (VSL: the primary way to reduce calculated surface slip) 10
3.3.1 Energy-absorbing layer 11
3.3.2 Shallow layer with different D_c 12
3.3.3 Slip rate dependent sliding coefficient 12
3.3.4 Depth dependent initial stress 13
3.4 Tests of multi-segmentation on ground motion (1Hz) 14
3.5 Tests of different dip angles 15
3.6 Tests of random initial stress contribution 16
3.6.1 1Hz result 16

4 Modeling multi-segment fault (subparallel planes) **16**
4.1 Tests of separation distances 16
4.2 Tests of initial stress tapering near the surface 17
4.3 Tests of overlapping distances 17
4.4 Tests of VSL 17

5 Modeling complex fault geometry **17**
5.1 Tests of the role of existence of tear fault 17
5.2 Tests of the role of complex fault geometry discretization 18
5.2.1 0.5 Hz ground motion comparison 19
5.2.2 0.25 Hz ground motion comparison 19
5.3 Simulations of 1Hz with complex fault geometry 19
5.3.1 Fault geometry without singular point (25 out of 26 pts) 19
5.3.2 Fault geometry with singular point but nucleates at south 19

1 Introduction and Overview

Approximately 80% of Utah's 2.7 million people live within 15 miles of the Wasatch Fault. This area is one of the most hazardous places in the US that under the threat of big earthquakes (M > 7). There are few strong motion records from normal faulting earthquakes all around the world. On the other hand, simulations of dynamic rupture processes provide an effective method for estimating ground motion due to potential big events. Our major work concentrates on the potential seismic hazard due to uncertainties in seismic source. The tool we are using for these studies is a 3D finite element code, which can handle heterogeneous velocity structure and non-planar fault geometry in general.

- We first considered simulating ground motion due to dynamic rupture on the Wasatch Fault Salt Lake City (WFSLC) segment with a simplified planar dipping fault embedded in the 3D Wasatch Front Community Velocity Model (WFCVM). We worked out a basic meshing scheme for the fault geometry and a way to integrate the 3D velocity model into our FEM simulations. We investigated the ground motion sensitivity to velocity structures—uniform, layered, fully 3D—with a simple uniform initial stress on the fault plane. We also considered other factors such as, hypocenter location, heterogeneous initial stress, and compared the consequent rupture processes through snapshots of slip as it developed on the fault during the rupture[1].

- At the 2010 SSA annual meeting, we summarized our simulation results for planar fault models of the WFSLC. We looked at the synthetic ground motions on east-west profiles and tried to link the characteristic of ground motion with underlying geologic structure—shear wave velocity, sediment thickness, etc. We also compared our simulation results with NGA predictions[2].

- We noticed that in our dynamic rupture simulations the highest final slip always appeared where the fault broke the free surface. That is contrary to our knowledge on slip distribution from source inversions, and it violates the observation of surface rupture of around 2m in SLC segment due to historic earthquakes (DuRoss et al., 2011). A reasonable solution to this problem is to introduce velocity-strengthening—instead of the more common velocity weakening on most of the fault—in the shallow part of the fault. The velocity strengthening extends to depths of 3-4km. We did sensitivity tests on different numerical schemes to implement velocity strengthening in the shallow layer[3].

- Taking notice of the non-planar feature of WFSLC, we moved forward to

[1] Earthquake Ground Motion for the Salt Lake City Segment of the Wasatch Fault

[2] Wasatch Fault: Salt Lake City Segment Ground-Motion Simulation

[3] Comparison of Proxies for the 'Velocity Strengthening' Zone at Shallow Depth and Their Effect on Rupture Dynamics

investigate the effect of complex fault geometry on rupture processes. We started modifying the fault model by first simplifying it as a discontinuous fault with two subparallel segments. We then investigated the possibility of rupture jumping from one segment to another during a dynamic rupture of two parallel normal faults. We illustrated the time-dependent Coulomb stress changes on sub-parallel faults to the main segment in order to study the triggering possibility. We studied several cases with various configurations of sub-parallel planes with different separation distances all with uniform or depth dependent initial stress models[4].

- At the 2011 Southern California Earthquake Center (SCEC) meeting, we showed results for the WFSLC as a non-planar curved fault with constant dip angle but with variations of the strike angle along strike. We updated our meshing scheme and extraction scheme for the velocity from the WFCVM accordingly. This made a more realistic model for the WFSLC. We noticed a sharp geometric singularity in the middle of the curved fault model. We investigated whether the seismic hazard was depended on the assumption of the fault continuity at this singular point (kink). We observed a non-symmetric triggering effect: if hypocenter were at north lower corner on the fault, the rupture would not propagate through the jump; however, if hypocenter were at south lower corner on the fault, the rupture would propagate through the jump. We developed a rather simple measure of the triggering ability depending on the intensity of Coulomb stress change on the targeted plane[5].

- Next we investigated how does the fault geometry implementation (roughness sampling) influence our ground motion and fault rupture process simulations. We used the fault trace data from the USGS and sampled the fault with a varying number of points, four through 26. The provided four different approximations of the WFSLC fault geometry with increasing degrees of geometrical complexities (smooth to rough fault model). We compared the ground motion response (PGV, CAV) by changing large-scale fault roughness. We also noticed that some rupture process might be influenced in a fundamental way, for example, a smooth fault model could rupture the entire length, but a rough fault model rupture might stops at the kink. This might be interesting to investigate because it most likely would impact the seismic hazard analysis. We presented our findings in the 2011 and 2012[6] Utah Earthquake Working Group (UEWG) meetings.

2 Model set-up

2.1 Plan view of the study area

Our study area is around the Wasatch Fault Salt Lake City segment (WFSLC) (Figure 1).

[4] Nucleation by Dynamic Triggering on a Multi-Segment Fault

[5] Does the Tear Fault Matter?

[6] Curved Dynamic Rupture Model For The Wasatch Fault SLC Segment

2.2 Finite element code

2.2.1. Fault plane construction

In the study of ground motion simulation of the WFSLC, we started with a planar fault model. We used the fault trace (Figure 1) and approximated the general strike direction as a straight-line (Figure 2).

In later studies when we will take into account the variation of the fault strike by directly using the fault trace data or using sampled fault trace data to model the fault. In all cases (simple strike direction or varying strike direction), we construct the fault surface in such a way that the fault has a constant dip of 50˚.

Figure 1: WFSLC area map view; red curve is WFSLC fault trace.

2.2.2 Mesh generation

The mesh is generated to comply with the fault surface model. Most of the meshing was done by first dividing the fault plane into grids, then extend the 2D surface grid along the horizontal direction which is perpendicular to the fault trace into a 3d grid. An illustration of the 3D meshing for planar fault models is in Figure 3, while you can get an idea of the 3D meshing for curved fault model from Figure 4.

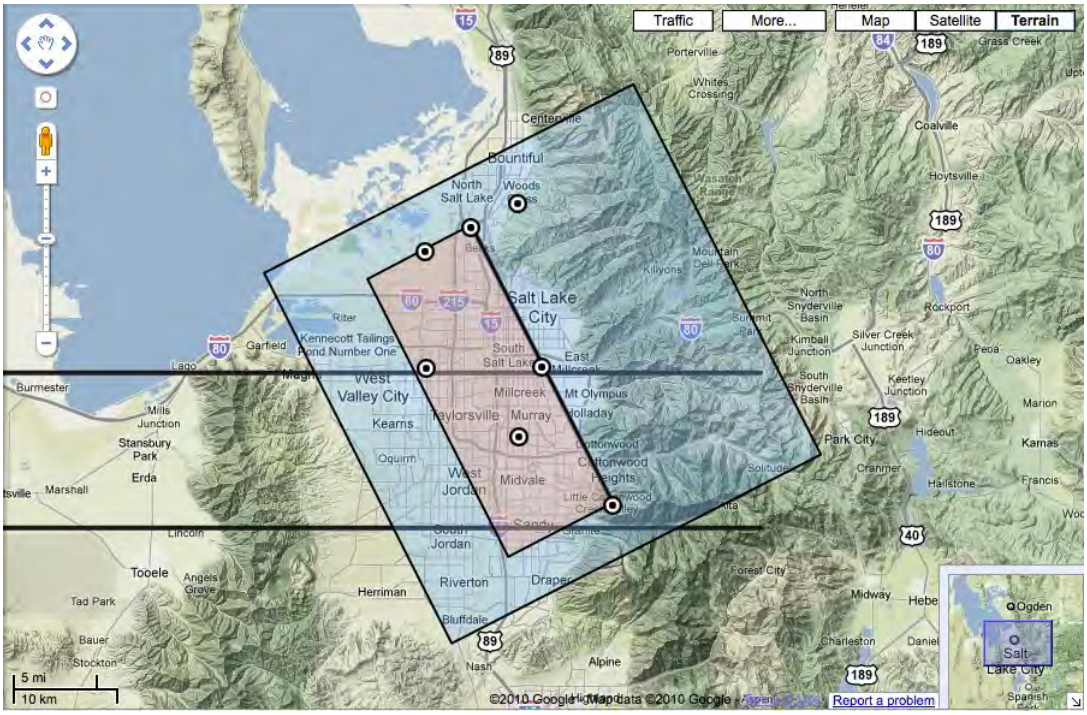

Figure 2: WFSLC map view with approximated fault trace

2.2.3 Incorporating WFCVM3.0

We use the Wasatch Fault Community Velocity Model version 3C (WFCVM3c) (http://geology.utah.gov/ghp/consultants/geophysical_data/zip/wfcvm_3c.tgz) to generate 3D velocity structure and incorporate it into our finite element simulations. Vp, Vs and Rho could be given at any specific geographic location using WFCVM3c program. We constructed the meshing first, in a local Cartesian coordinate system, in which fault is roughly going north to south. We then convert the grid points in the meshing into Geographic Coordinate system (lat,lon,dep) and then retrieve the material properties at the coordinates of each grid point. We use the value from one corner of each 3d hexagonal element as the physical properties for this element. General look at the CVM we are using is shown in Figure. 3.

2.2.4 Main parameters set-up

We used a 3D finite element code (Ma & Liu, 2006) with the ability of modeling complex fault geometry. The code is 2nd order accurate in space and uses 1-point integration in time. We currently don't include cohesion in our model. We used uniform normal stress distribution though sometimes we use a depth-dependent distribution as well. Based on the normal stress we calculate the initial shear stress along downdip direction using the static coefficient of friction of the initial stress $\mu 0$. For some cases we have included random perturbations on shear stress. We keep dynamic parameters such as D_c, μ_s, μ_d uniform over the fault plane, except the rupture initiation patch. In the initiation patch we simply elevated the initial stress to a level slightly higher than the yield stress (1.01 times yield stress) and adjust the dynamic parameters in the patch so that we can get final slip in the patch not too much different from what we get

at the other places of the fault.

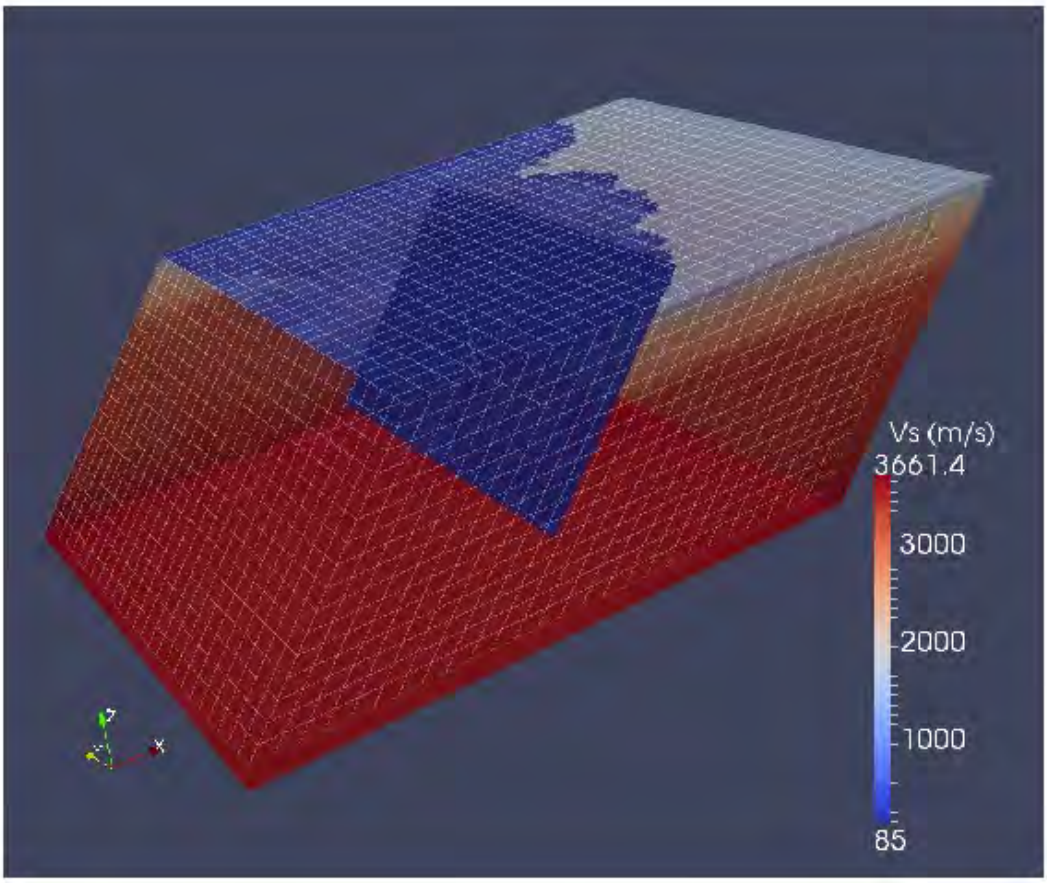

Figure 3: 3D meshing of planar fault model. Colors indicate value of shear wave velocity from the WFCVM.

3 Modeling a single fault

Dynamic rupture modeling is a highly complex calculation process involving a large number of parameters that must be specified: initial stresses, velocity structure, meshing scheme, friction law and its relevant parameters. Before proceeding to the major simulations, we conduct a number of tests to ensure that the set-up and parameters we use in the simulations are reasonable and accurate.

3.1 Tests of healing parameters

In the dynamic simulations with simple slip-weakening friction relationship, we observe elongated tails in the slip-rate function on the fault. The reason is that slip-weakening law does not contain any information about fault healing, which is a physically reasonable process since the fault is going to regain its strength to a certain level after it stops sliding (even if for just a moment). Omitting the healing mechanism in slip-weakening relationship produces a lot of small amplitude reverberations after the biggest slip-rate pulse. To play against it, we implemented healing mechanism in the realm of slip-weakening law. We simply change the friction coefficient so that it regains part of the strength when the fault stops sliding.

$$\mu_S = \mu + (\mu_S 0 - \mu) * healingCoef$$

where $\mu_S 0$ is the initial static coefficient, μ is the sliding coefficient, μ_S is the static coefficient after the point stops sliding, *healingCoef* is the percentage of strength it regains after the point on the fault stops moving.

We tested several cases with *healingCoef* equaling to 0 (no healing), 0.1, 0.2, 0.3, 0.5, 1.0 (full healing). We found that for practical use, 0.5 is a reasonable value that could be used to eliminate the trailing noise of slip-rate function due to the healing.

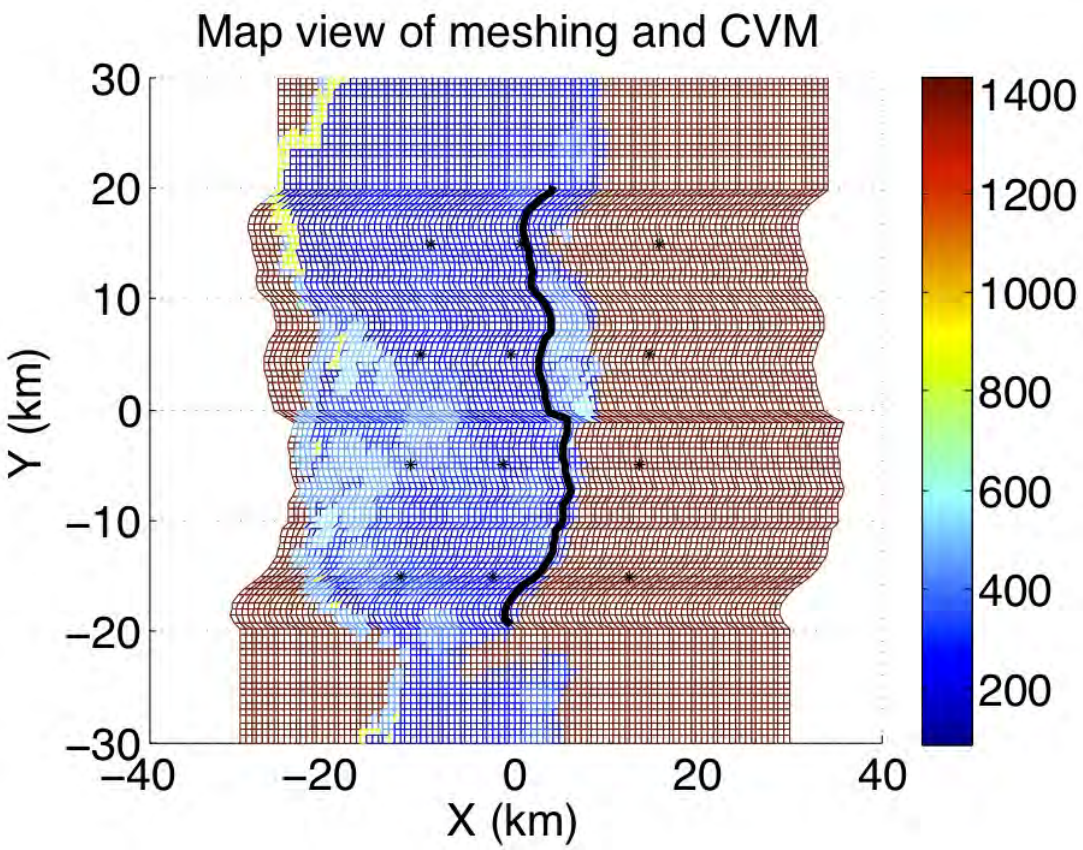

Figure 4: 2D map view (free surface) of 3D meshing of curved fault model.

3.2 Tests of shallow layer stress tapering (one way to reduce surface calculated offset)

A major challenge was to make the calculated surface slip consistent with geologic observations (surface slip up to around 2m for historic events, DuRoss et al., 2011). For a target earthquake magnitude,e.g. Mw 7.0, we always had the largest slip near the free surface in our simulations with uniform initial stress. The situation didn't improve much when we changed to a depth dependent initial stress model. In order to solve this problem, we tried to reduce the surface slip by introducing stress tapering at very shallow depth (0-3,4km) in our uniform initial stress model. An example of stress tapering to different depths is shown in Figure 5, with their corresponding slip spatial-temporal distribution along the symmetry line along dip on the fault plane in Figure 6. As seen from the comparison, initial stress tapering is one way to reduce large slip near the free surface.

Table 1: Basic parameters

Lx,Ly,Lz	40km, 40km, 17km
dx,dy,dz	50m,50m,50m
strike,dip	153, 50
Friction law	Slip weakening
Initial normal stress	36MP
a	
$\mu 0, \mu d, \mu s$	0.55, 0.448, 0.66
Dc	0.25m
Tmax	30sec
Vs minimum	500m/s
Maximum Freq	1Hz

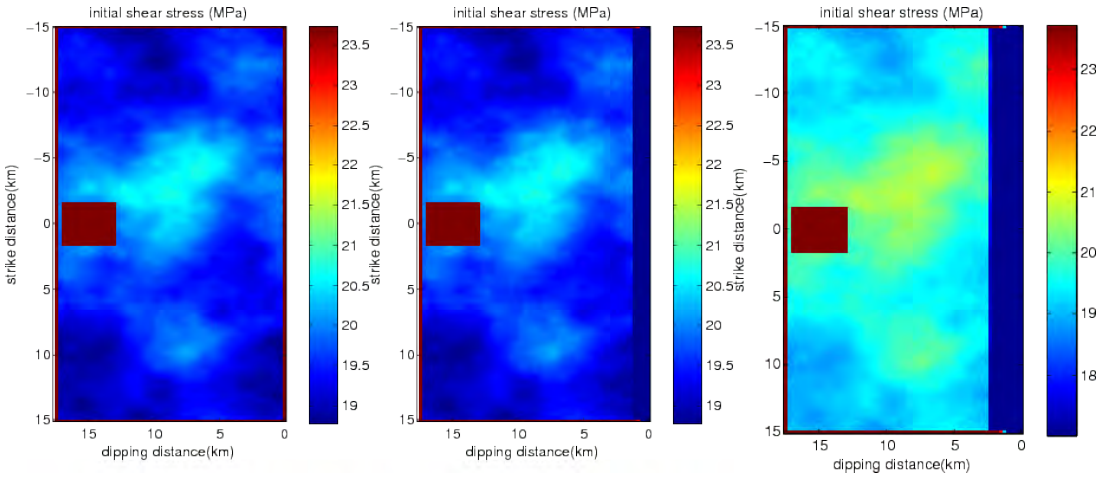

Figure 5: Initial stress for 0km (no), 1km, 2km tapering (left to right)

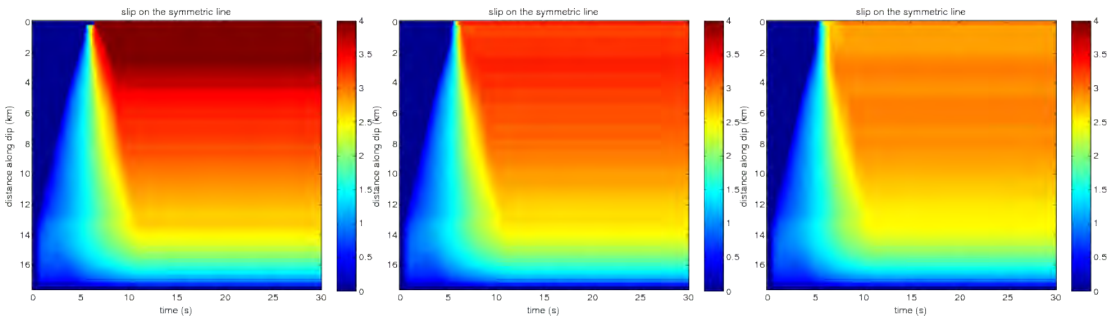

Figure 6: Final slip for 0km (no), 1km, 2km tapering (left to right)

3.3 Tests of shallow layer velocity strengthening (VSL: the primary way to reduce calculated surface slip)

We did a systematic analysis of different implementations of velocity strengthening behavior in the top 3–4km layer in our finite element model with the slip-weakening friction relationship. We analyzed the effect of reducing near surface fault slip and the large amplitude ground motion by each method to identify the sensitivity area for the key parameters in each formulation. Here we

document the results from analyzing four different implementations of velocity-strengthening layer (VSL).

Overall, the first three implementations work in quite similar ways. They all help reduce the near surface fault slip and therefore the ground motion. We plot peak ground velocity (PGV) along four profiles that cross the fault at different latitudes (Figure 7). In Figure 8 we compare PGV among the models: no VSL is black; 2km VSL with $\mu d0$=0.6 is red; and 2km VSL with $\mu d0$=0.55 is blue.

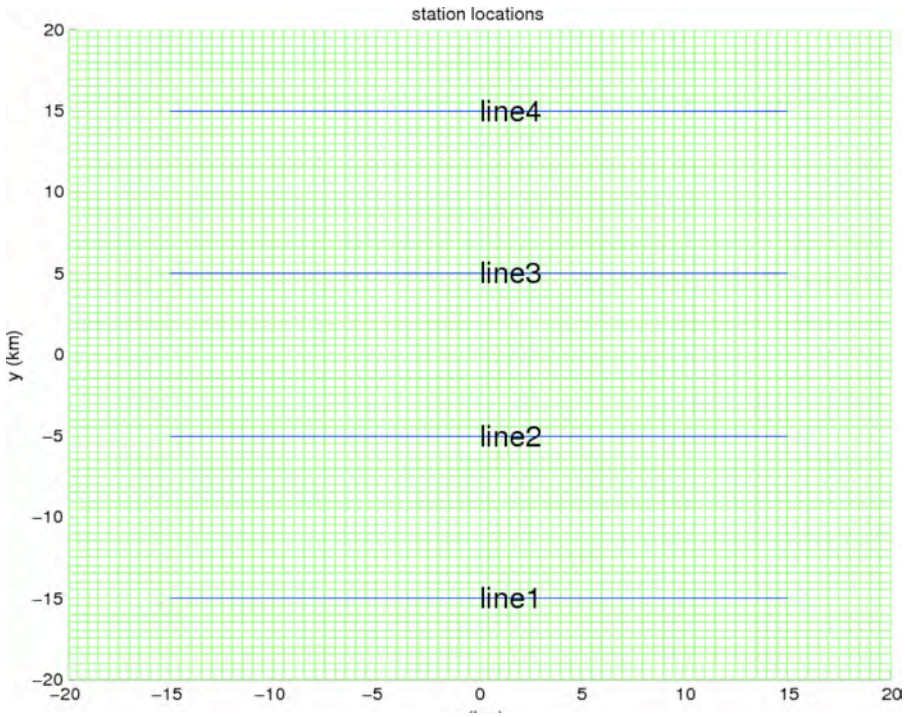

Figure 7: Profile locations

3.3.1 Energy-absorbing layer

$$\mu d = \mu d0 \quad (z < dp)$$

$$\mu d = 0.448 \quad (z >= dp)$$

Here μd is the sliding friction coefficient, 0.448 is the value we used for μd for most of the fault, while we change the μd to some other value when at shallow depth. Here z is depth while *dp* is the thickness of the velocity strengthening layer (VSL).

In this implementation, the main parameters are *dp* and μd0. Figure 9 shows the comparison of fault slip and ground motion statistics with different combinations of parameters *dp* and μ*d*0. Noticed that those profiles are all central lines either along dip on the fault or on the free surface perpendicular to the fault. We will get, especially near the free surface. The maximum sliprate tends to scale with *dp* in the same way except that the impact is almost concentrated at the top couple of kilometers near the free surface. The ground motion will change accordingly as the sliprate and slip changed on the fault. When we change μ*d*0, we observe similar variations of fault. When we change the *dp*, we can see the thicker VSL we have, the lower amount of slip slip and ground motion statistics as we change *dp*.

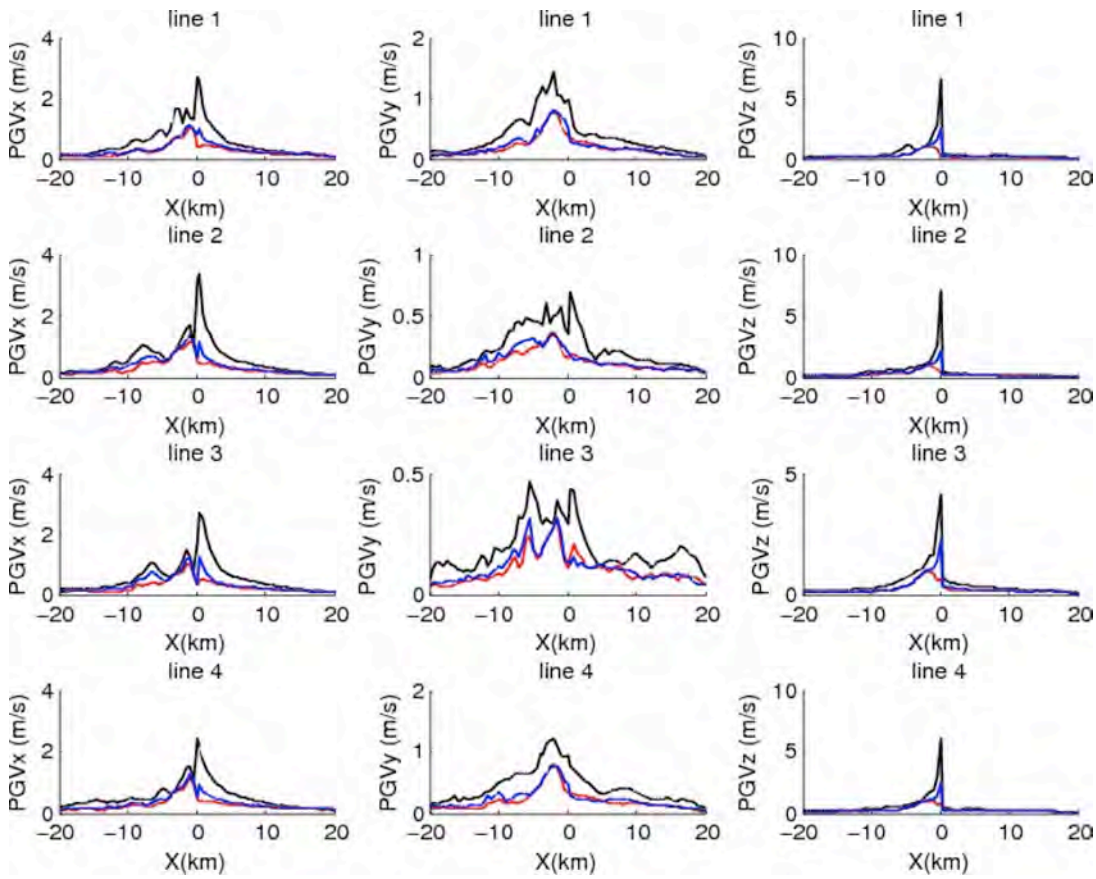

Figure 8: Comparison of ground motion with/without VSL.

3.3.2 Shallow layer with different D_c

$$D_c = D_{c0} \quad (z < dp)$$

$$D_c = 0.25 \quad (z >= dp)$$

D_c is the critical distance in slip-weakening formulation. D_{c0} is the value of D_c in the VSL. A similar sensitivity test result as shown in the previous section is shown in Figure 10.

3.3.3 Slip rate dependent sliding coefficient

$$\mu_d = 0.448 + (\mu_s - 0.448) * Vr/Vrlim \quad (z < dp)$$

$$\mu_d = 0.448 \quad (z >= dp)$$

Here we simply make μ_d linearly scale with slip rate. One consequence one would expect from this implementation is that after sliding for D_c distance, the point of the fault will have sliding friction totally dependent on its current slip rate. Parameter sensitivity result is shown in Figure 11.

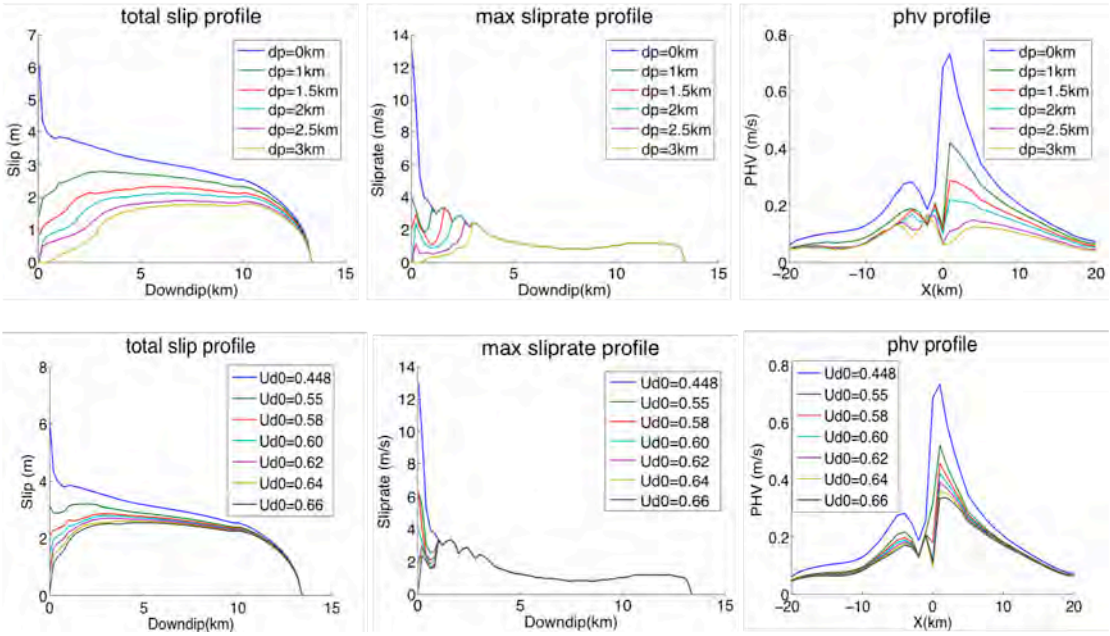

Figure 9: Result of Implementation 1

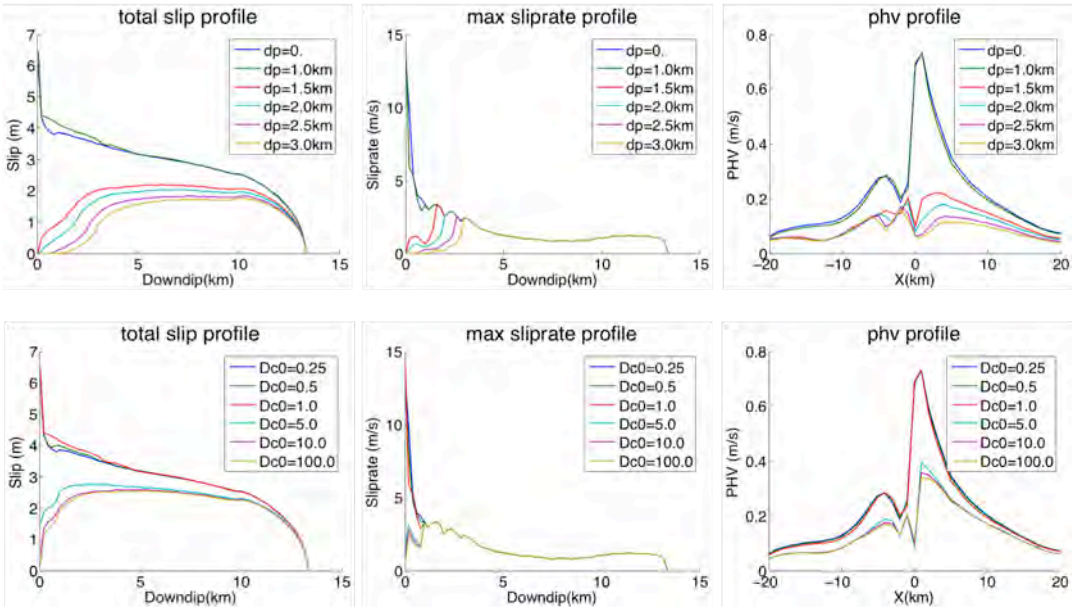

Figure 10: Result of Implementation 2

3.3.4 Depth-dependent initial stress

$$\mu d = \mu d0 \quad (z < dp)$$
$$\mu d = 0.448 \quad (z >= dp)$$
$$\sigma = (\rho - 1000.)gh * Cos(dip)$$

Similar to implementation 1, here we are using a depth dependent (linear increasing with depth) initial stress condition. σ is the initial effective normal stress, dip is the dipping angle of the fault, ρ is the average density, 1000 is the density of water. What is different from previous implementations is that,

because the initial stress is increasing with depth, the major slip and sliprate are in the deeper part of the fault, which makes the VSL less effective (Figure 12).

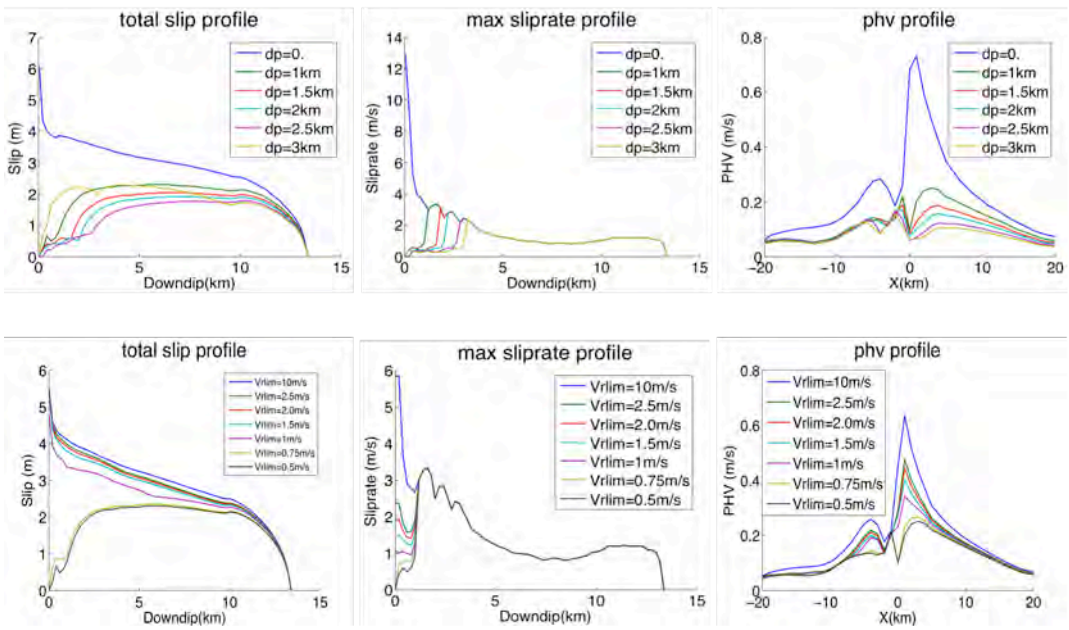

Figure 11: Result of Implementation 3

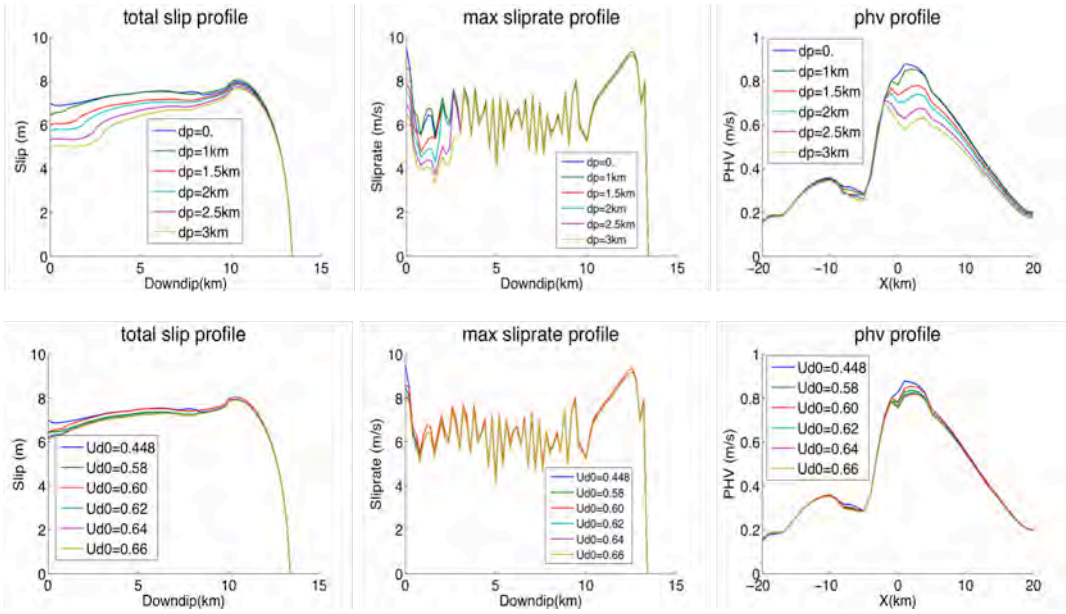

Figure 12: Result of Implementation 4

3.4 Tests of multi-segmentation on ground motion (1Hz)

Up till now we are only considering the earthquake scenario due to a planar normal faulting simplified from fault trace data. Here we would like to take into account the consequence of multi-segmentation of the fault. We assume that the two segments are co-planar and they are separated by 1km step-over. Slip from a seismic source that is a single fault dynamic rupture and a two-segment fault dynamic rupture look are shown in Figure 13. To illustrate the effect of multiple-segments we show PGV for the 4 lines in Figure 7 resulting from a single-plane and a two-plane fault (Figure 14).

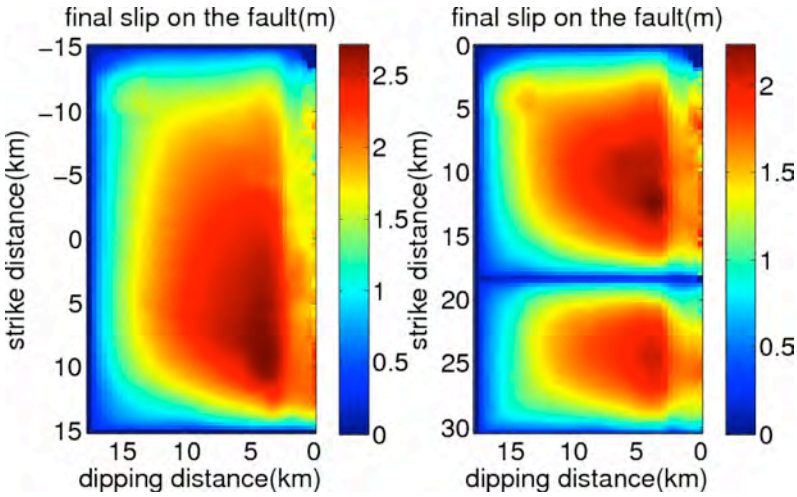

Figure 13: Single fault (left) and two-segment (right) rupture final slip.

3.5 Tests of different dip angles

One of the very first tests we have done is to experiment with different dipping angles. It is generally believed that the dipping angle of the Wasatch fault is 50° with variations from segment to segment. To test the sensitivity of different dipping on our earthquake simulations, we model dynamic rupture process with uniform initial stress distribution under various dipping angles (45, 50, 55, 60 degree). The results showed there's no significant difference in terms of fault rupture process or ground motion statistics.

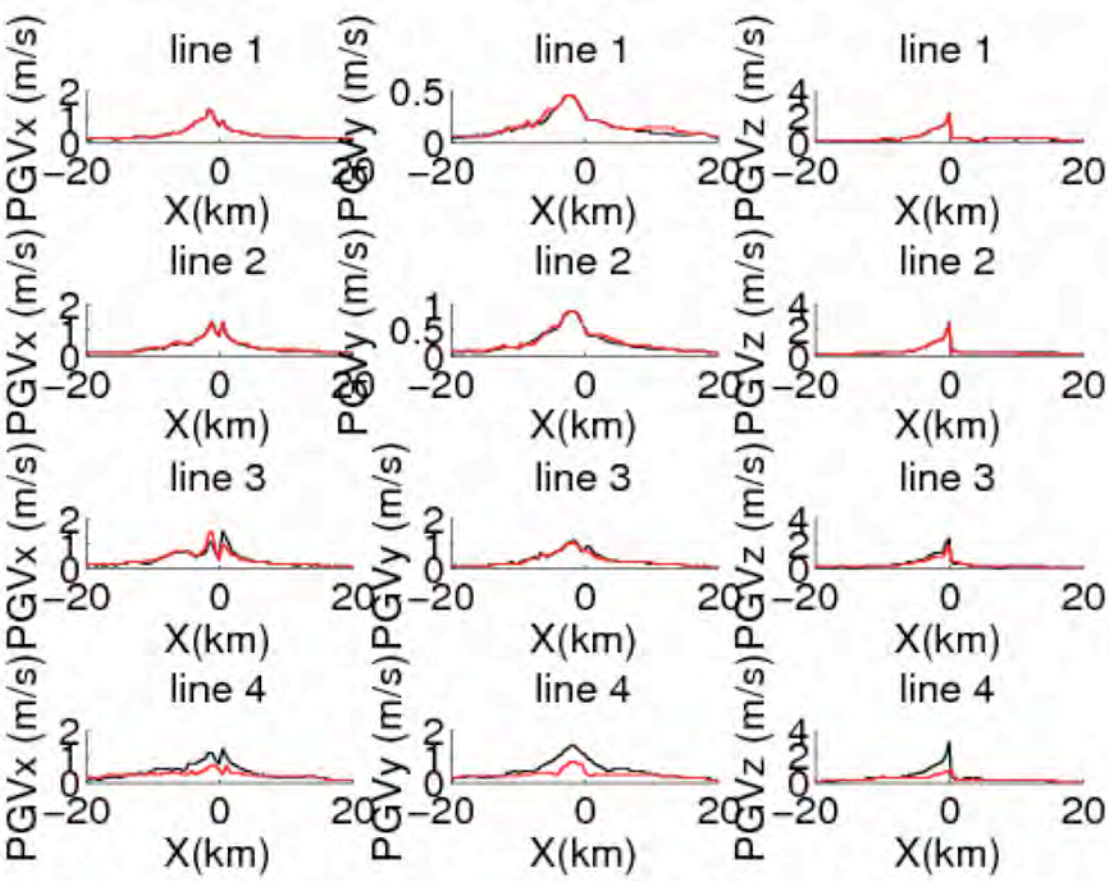

Figure 14: Comparison of ground motion for single/multiple fault (Single fault plane result is shown in black while multi-segment fault result is shown in red.)

3.6 Tests of random initial stress contribution

3.6.1 1Hz result

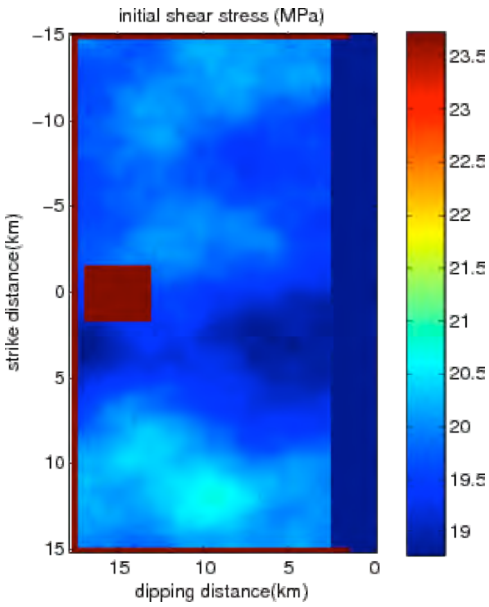

Figure 15: Case 1: Initial shear stress.

Here we show two examples of our low-frequency ground motion simulations (up to 1Hz) with planar fault models. Notice that the initial stress is tapered to zero to the free surface in the shallow 2km layer to reduce the potential unrealistic amount of surface slip. Case 1: A bilateral rupture without perfect symmetry due to initial stress randomness (Figure 15) with the resulting ground motions at various stations across the valley (Figures 16, 17, 18, and 19). Case 2 is another example of the effect of the initial stress distribution (Figure 20) with the resulting ground motions shown in Figures 21, 22, and 23.

4 Modeling multi-segment fault (subparallel planes)

Here we investigate the consequences of possible multi-segmentation of WFSLC to the potential ground motion and seismic hazard in a more systematic way. We have already shown that whether the fault is a continuous planar one or with a small step in the middle will make a significant difference in terms of ground motion. Here we take into account how the result will be affected by possible segmentation characterized by two parameters, stepover distance and overlapping distance (see Figure 24), which are commonly used in multi-segment dynamic rupture studies. Geologic observations are limited to near surface and with large uncertainties. Thus considering these uncertainties and understanding their consequences are important to hazard estimation and analysis.

4.1 Tests of separation distances

Because of the complexity of the problem, we decided to test with a simple homogeneous velocity structure rather than the 3D WFCVM. We tested cases with changes less than 1km overlapping distance to see if the rupture could jump a gap with a certain level of separation distance. Our tests show, under the specific uniform stress condition we have on both segments of the faults, the rupture could not jump a separation distance larger than 2 km.

Generally speaking, even in a simple case of two, sub-parallel segments, the jumping distance will vary according to the configuration, e.g. initial stress conditions on the two segments, velocity structure being used, whether there is a nucleation patch on the to be triggered segment (high initial stress patch), separation distance and overlapping distance between two segments. Most of the existing research on jumping dynamic ruptures focuses on the geometrical factors

such as separation and overlapping distances. It reflects the limitation of observations and also leaves a lot of potentially interesting research areas to study.

4.2 Tests of initial stress tapering near the surface

While geological observations of slip are primarily constrained to the near surface, it is unlikely that the largest amount slip occurs near the free surface. Here we examine whether the stress tapering near the free surface, which is one way of reducing near surface slip amplitude, will influence the rupture jumping behavior. We used a homogeneous velocity structure with separation distance of 1km and an overlapping distance of 1km. We tested three cases with different tapering depth: 1km, 2km and 4km. Overall as we increase the tapering depth, we observe the major slip area moving from near surface towards the center of the fault, but we didn't see much difference in terms of timing of triggered rupture or the nucleation location of the triggered rupture. The three cases look similar in terms of dynamic triggering effect.

4.3 Tests of overlapping distances

Our reference model for overlapping distance analysis is simple. We use a homogeneous velocity structure and a uniform initial stress with stress taperering in the upper 2km; separation distance is 1km. We tested overlapping distances of 2km, 0.5km, 0km, -1km, -2km (negative overlapping distance simply means there is gap between the corresponding fault boundaries of the two segments. As long as the two segments have positive overlapping, we don't see much difference in triggering rupture process. But as we pull them farther away, the triggering possibility decreases, and we see delayed triggering in the case of -1km. The rupture never jumped to the second segment in the case of an overlapping distance of -2km.

4.4 Tests of VSL

Compared to stress tapering, the VSL has much stronger effect on reducing peak slip and peak slip-rate as well as making rupture jumping from one segment to another less probable. We used stress tapering within the shallow 2km and use an energy-absorbing VSL implementation (with μd=0.55). When we use separation distance of 1km, we couldn't make the rupture go through the gap regardless of the overlapping distance. Only when we further reduce the separation distance to 0.5km was the rupture able to trigger rupture on the second segment. Interestingly, because of the VSL, the nucleation point of the triggered segment moved deeper toward the central part of the fault, closer to the expectation we would have for a natural event. This might have implications for the multi-segment earthquake rupture studies. If the velocity-strengthening layer is physically meaningful, then we might expect a separation distance threshold smaller than that (4km) described in the previous studies.

5 Modeling complex fault geometry

5.1 Tests of the role of existence of tear fault

We investigated the role of the potential tear fault in WFSLC in 2011 SCEC

Annual meeting.

Since the tear fault (Figure 25) makes an abrupt change of fault geometry in the middle of WFSLC, we want to see if it makes a difference with and without the linking of the north and south portion of the WFSLC in terms of the dynamic rupture process on the curved fault. We used the full 26pts of fault trace data from USGS database to construct the fault geometry model and make the finite element meshing accordingly. The model set-up is almost the same as previous cases except the fault geometry and consequently meshing.

- the simulation result simply shows that under the parameters we used in the simulation (especially the uniform initial stress condition we used) the rupture can not jump from north section to south section without the tear fault (Figure 26). in other words, the continuity of fault is required to have the whole WFSLC ruptured in one earthquake (when hypocenter is in the north as in Figure 27)
- In order to consider measuring and estimating the triggering from one fault segment to another, we developed a simple proxy. The proxy is a characterization of the temporal and spatial distribution of Coulomb stress change on the target fault section near the fault discontinuity (Figure 28). 2 ways we tried to feature the Coulomb stress field:
  1. for a certain threshold, find the area where the maximum temporal Coulomb stress change exceeds that threshold (static method)
  2. track the largest area where the Coulomb stress change exceeds the threshold at every time step (dynamic method)

  we make one section of the fault rupture (master fault) while preventing the other section (slave fault) from sliding, and then measure the Coulomb stress change on the slave fault.

  By using the TA curve (curve of the area as a function of its corresponding threshold) we were able to confirm the following questions:
  - rupture from south more easily triggers a through-going rupture than the ones from north (case CUR13 vs CUR11)
  - it is easier for the rupture to jump to the other section when the hypocenter is farther from the tear fault (case CUR14 vs CUR11)
  - the higher the initial stress level (smaller S factor), the higher triggering ability it has (see case CUR16(S=1.47) CUR11(S=1.10) and CUR15(S=0.87))
  - we fix the initial stress on northern part (master fault) the same while using different levels of initial stress on the southern part, we get similar results on the stress level which could trigger the southern part to rupture, from numerical tests and TA-curve predictions. this could be used as a show case of the potential usage of TA-curve in calculating and predict the critical stress level of triggering multi-segment rupture.

5.2 Tests of the role of complex fault geometry discretization

for full description of the project, see folder Curved

We get the fault trace data from USGS website, we select part/all of them as the dataset, and construct the numerical fault trace out of those points (by linear

interpolation between adjacent points). We then pave the numerical fault trace curve along the 50 degree down-dipping direction and thus make the whole dipping fault with almost uniform dipping angle and non-uniform strike angle along the strike. In this way we made four different configurations of fault geometries (with roughness on different scales), identified by the number of data points we used from the original USGS fault trace data. They are shown in Figure 29:

1. full 26pts (model A)
2. 2pts (model B)
3. 4pts (model C)
4. 8pts (model D)

5.2.1 0.5 Hz ground motion comparison

We calculated the rupture process as well as the ground motion at selected stations for fault model A B and D (hypocenter in the north). The cases are AGU06 AGU07 and AGU08. we found that with the most complete fault model A, the rupture could not get through the kink (Figure 30). We also calculated another AGU09 for different hypocenter locations to AGU06, and this time, the rupture goes through the kink from south to north. This result is pretty similar to the ability to jump from our results from AGU 2011.

5.2.2 0.25 Hz ground motion comparison

We don't have any difficulty in having the rupture going through the whole fault in any of the 0.25 Hz cases. For model A B C and D we have case YUL00 YUL01 YUL02 YUL03, with uniform initial stress conditions. We also tried depth-increasing initial stress conditions with model A and B.

As the fault geometry models gradually changes (Figure 31), we can see consistent ground motion statistics patterns of PHV and CAV, although the details of the final slip on the fault near those geomet- rical singularities become heterogeneous. Also the depth-dependent cases show similar overall features as in the uniform initial stress case.

5.3 Simulations of 1Hz with complex fault geometry

5.3.1 Fault geometry without singular point

Case UTH01_triton: In the previous sections on 0.5Hz simulations, we showed that the rupture could not go through the kink in the middle of the WFSLC based on the most complete fault geometry model we have. Thus we made adjustment to the fault geometry model and smooth the kink. We carry on dynamic rupture simulations based on this modified fault geometry model. The rupture propagates across the entire fault (Figure 32). Waveforms at selected stations (Figure 33) are shown in Figures 34-36.

5.3.2 Fault geometry with singular point but nucleates at south

Case UTH02_triton: We calculated an earthquake scenario with seismograms good to 1Hz with the non- modified fault geometry model (with the kink). The earthquake initiates at the south end and rupture unilaterally to the north. The final slip distribution of this run can be found in Figure 37.

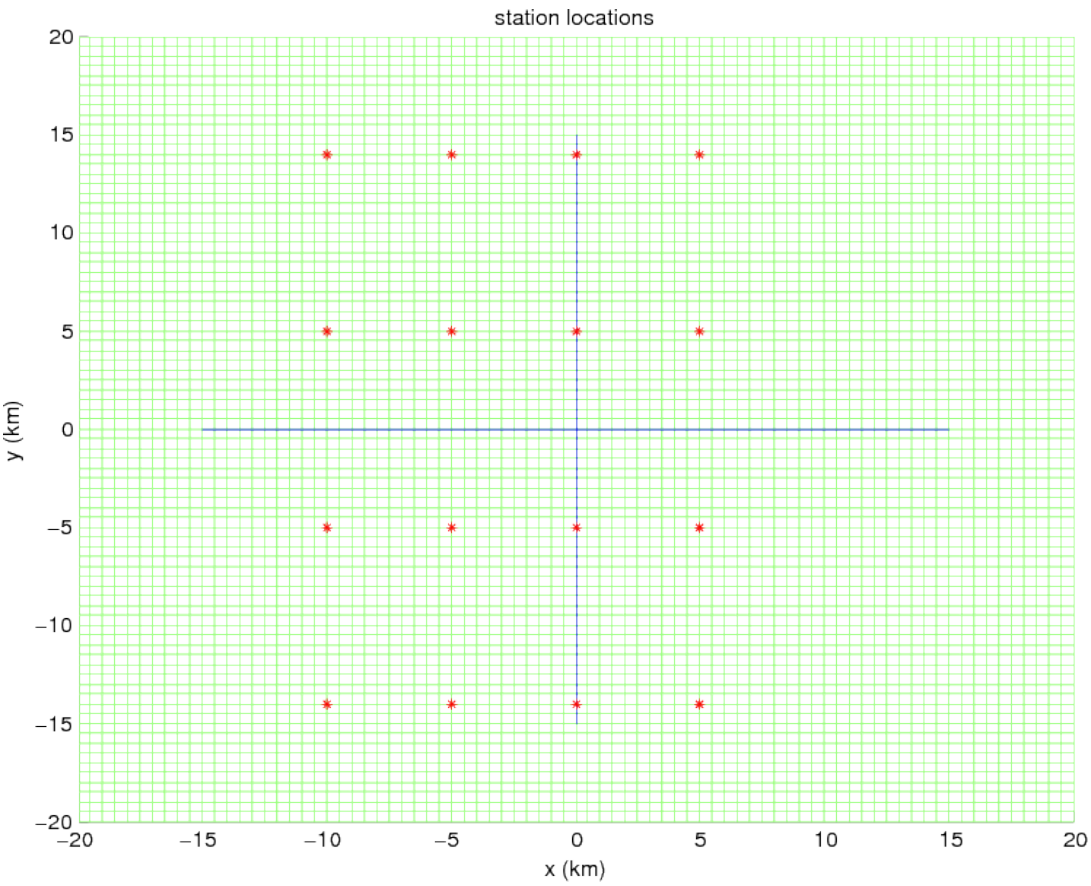

Figure 16: Station map.

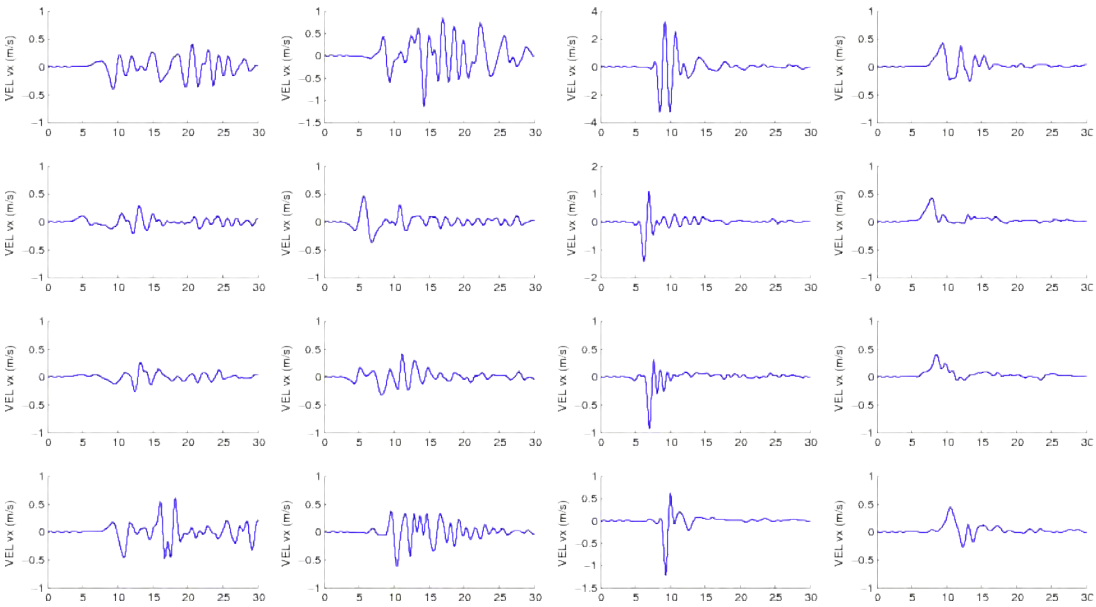

Figure 17: Case 1: East-West (X) component seismogram

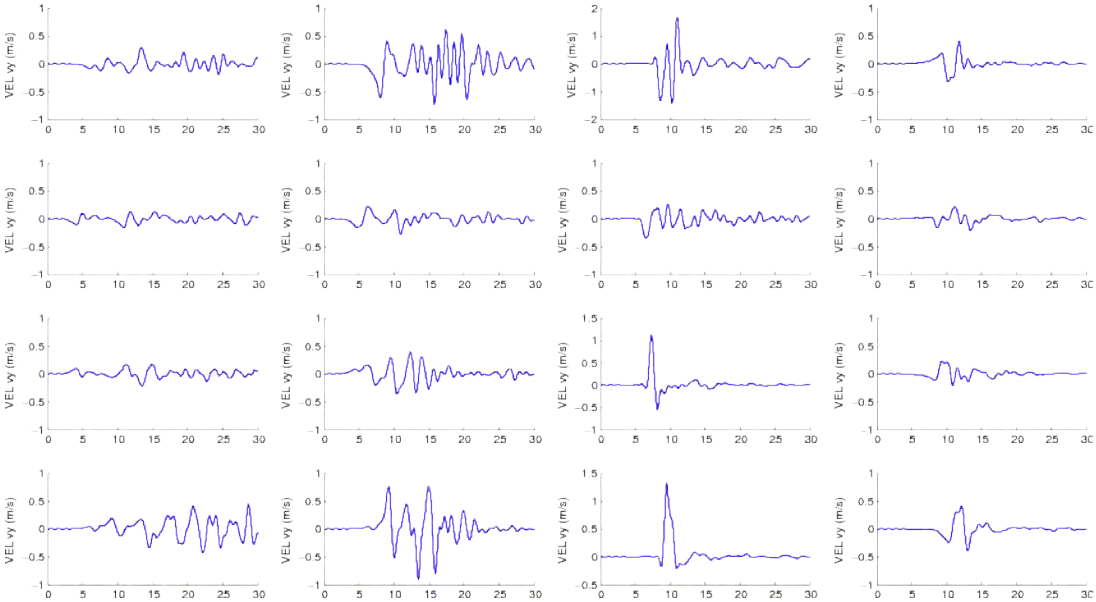

Figure 18: Case 1: North-South (Y) component seismogram.

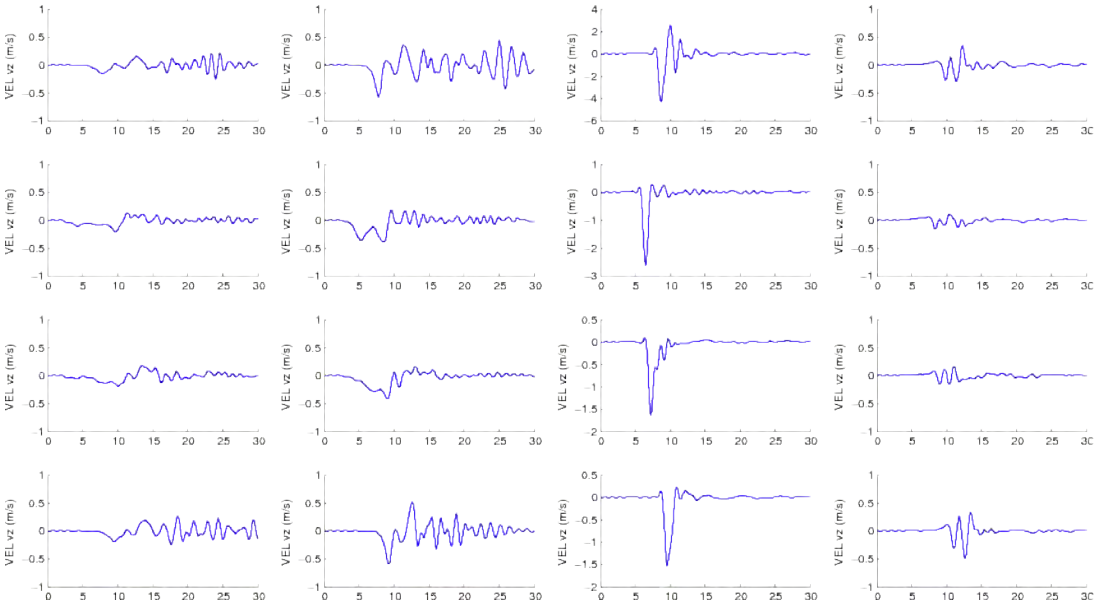

Figure 19: Case 1: Vertical (Z) component seismogram.

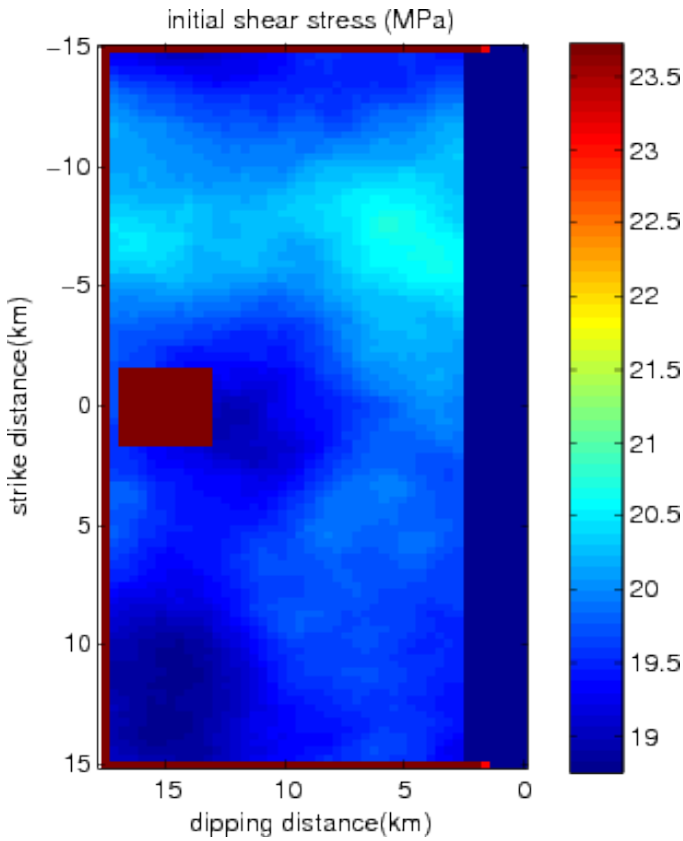

Figure 20: Initial shear stress for Case 2.

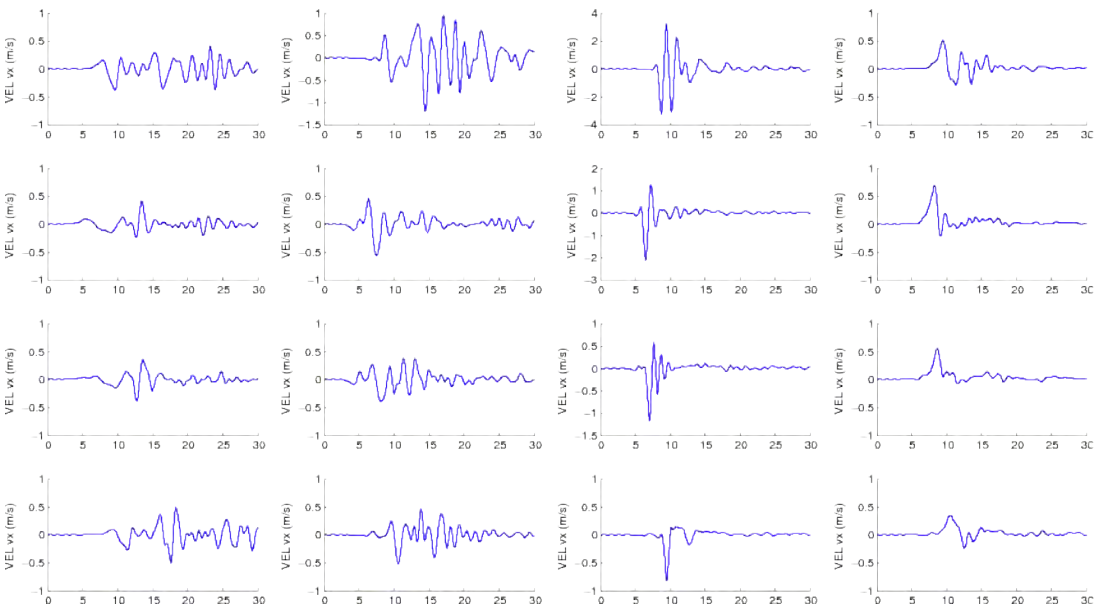

Figure 21: Case 2: East-West (X) component seismogram

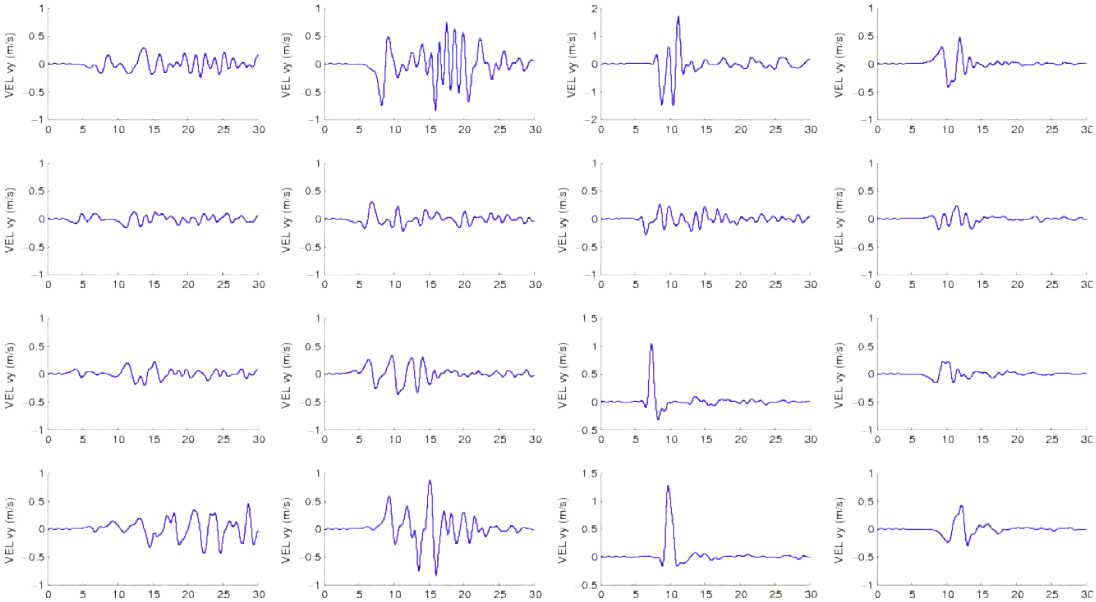

Figure 22: Case 2: North-South (Y) component seismogram.

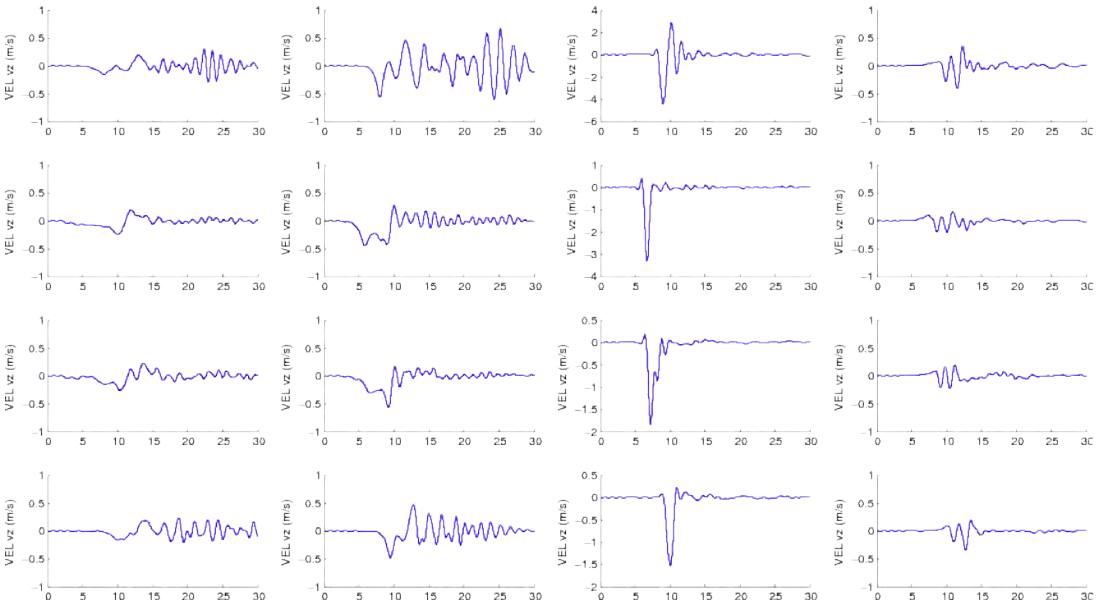

Figure 23: Case 2: Z component seismogram.

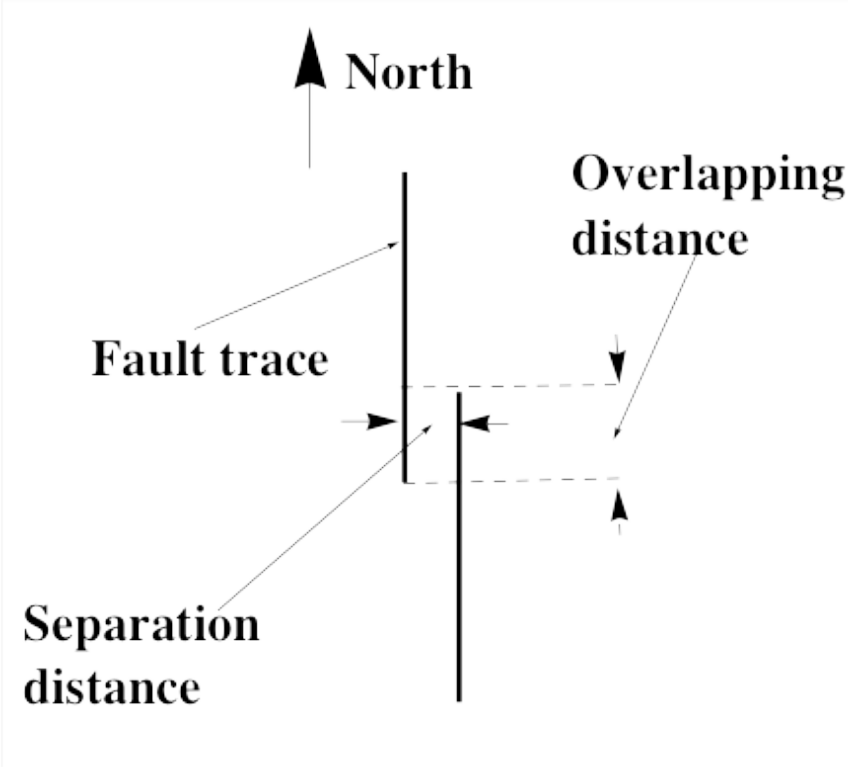

Figure 24: Definition of separation and overlapping distance.

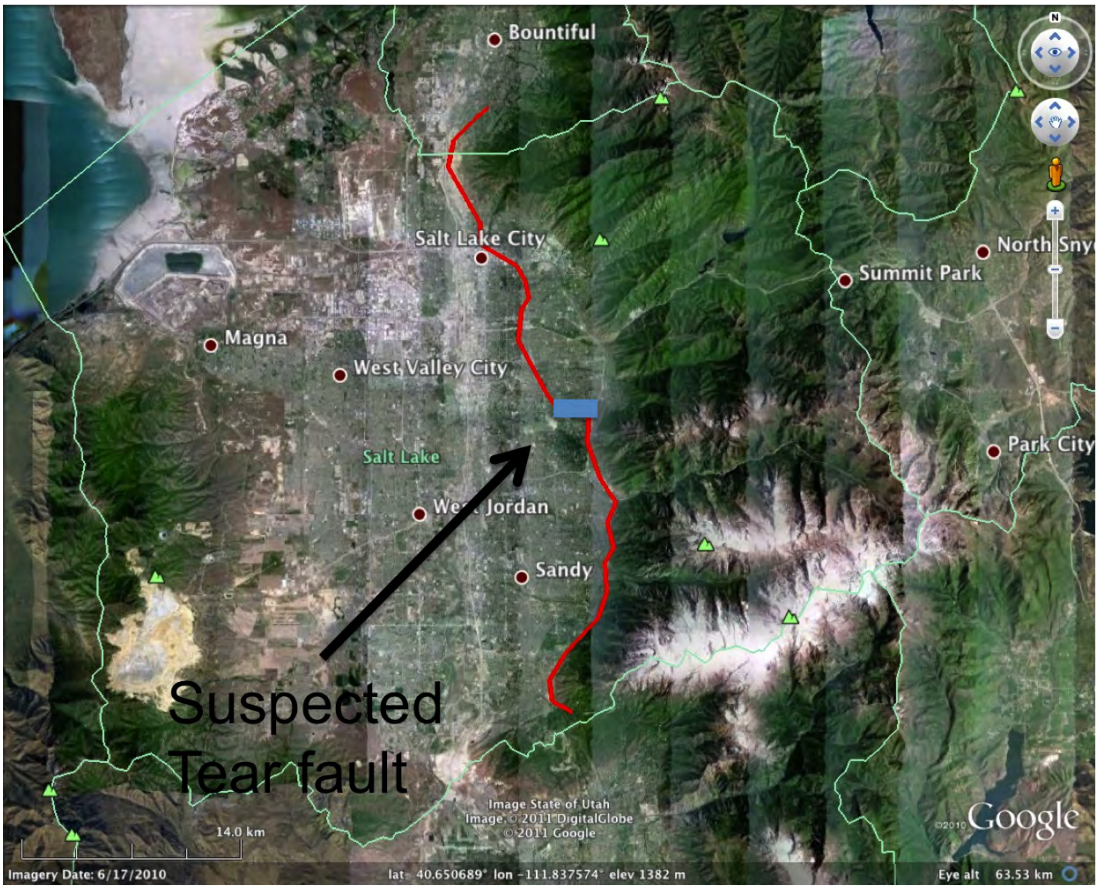

Figure 25: Suspected Tear Fault location in WFSLC.

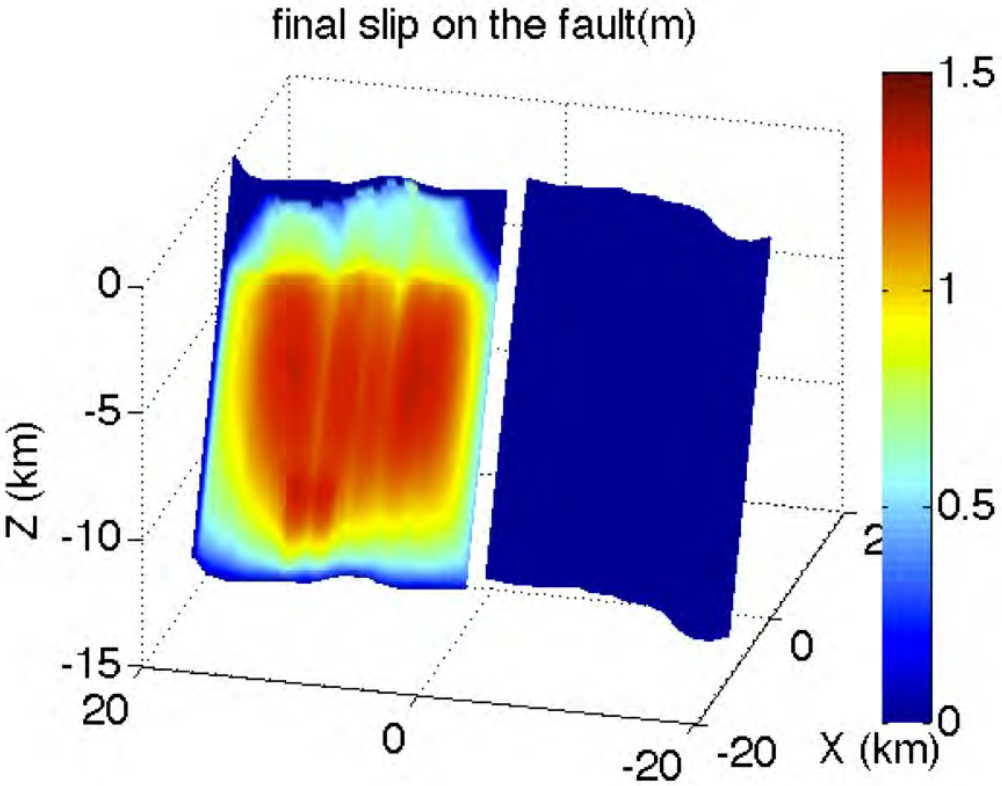

Figure 26: Final slip in the simulation with tear fault.

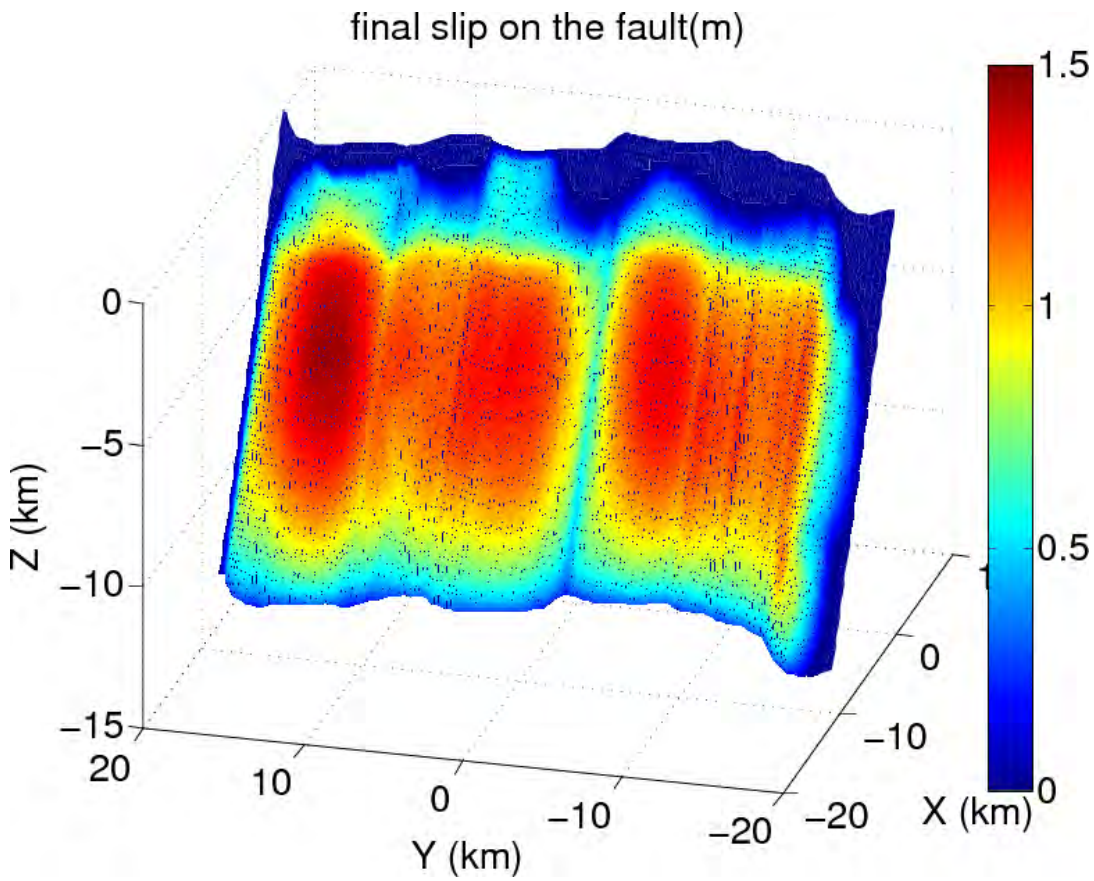

Figure 27: Final slip in the simulation without tear fault.

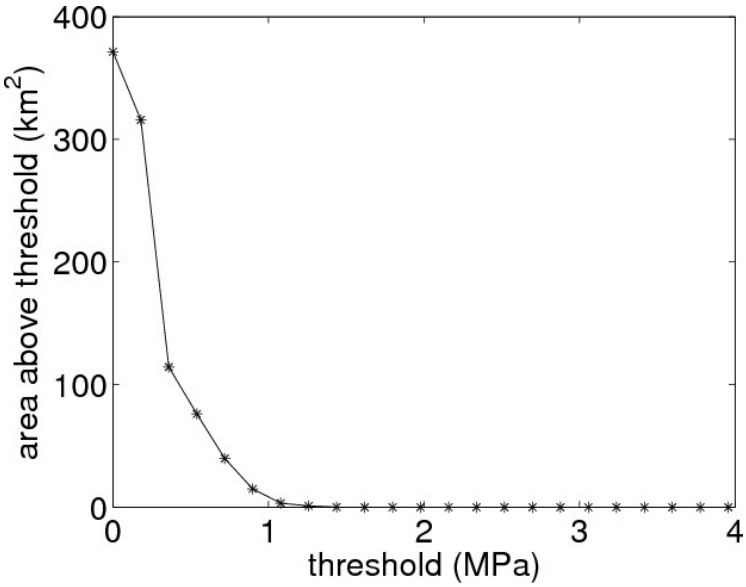

Figure 28: Example curve of the area as a function of its corresponding threshold (TA curve)

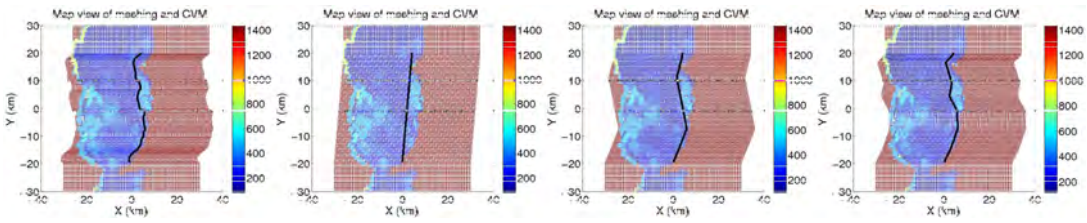

Figure 29: Model A-D (left to right) of fault trace discretization.

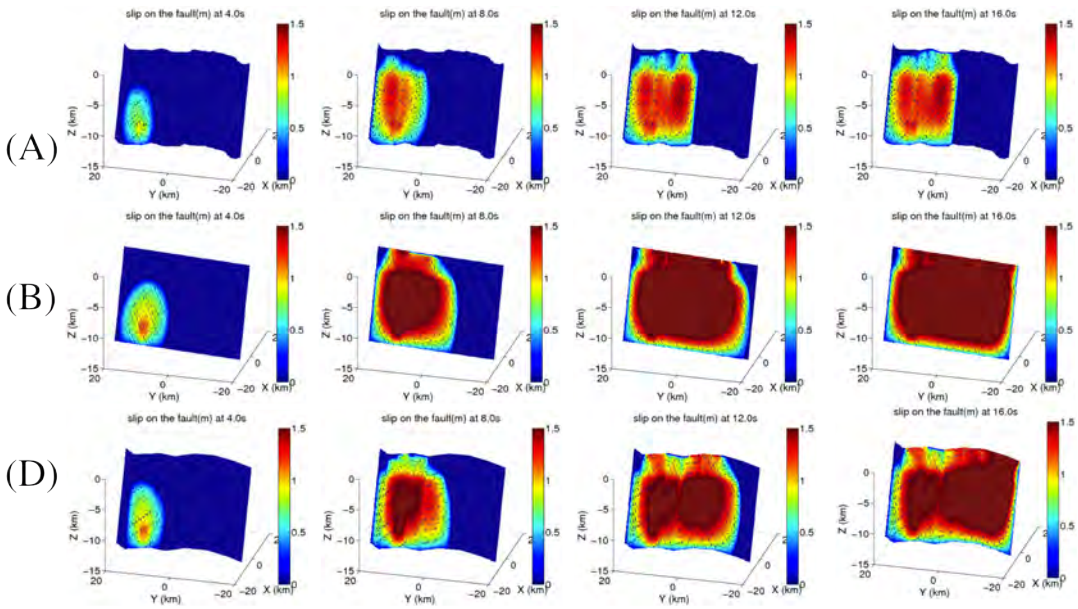

Figure 30: Rupture process snapshots for fault models A, B and D.

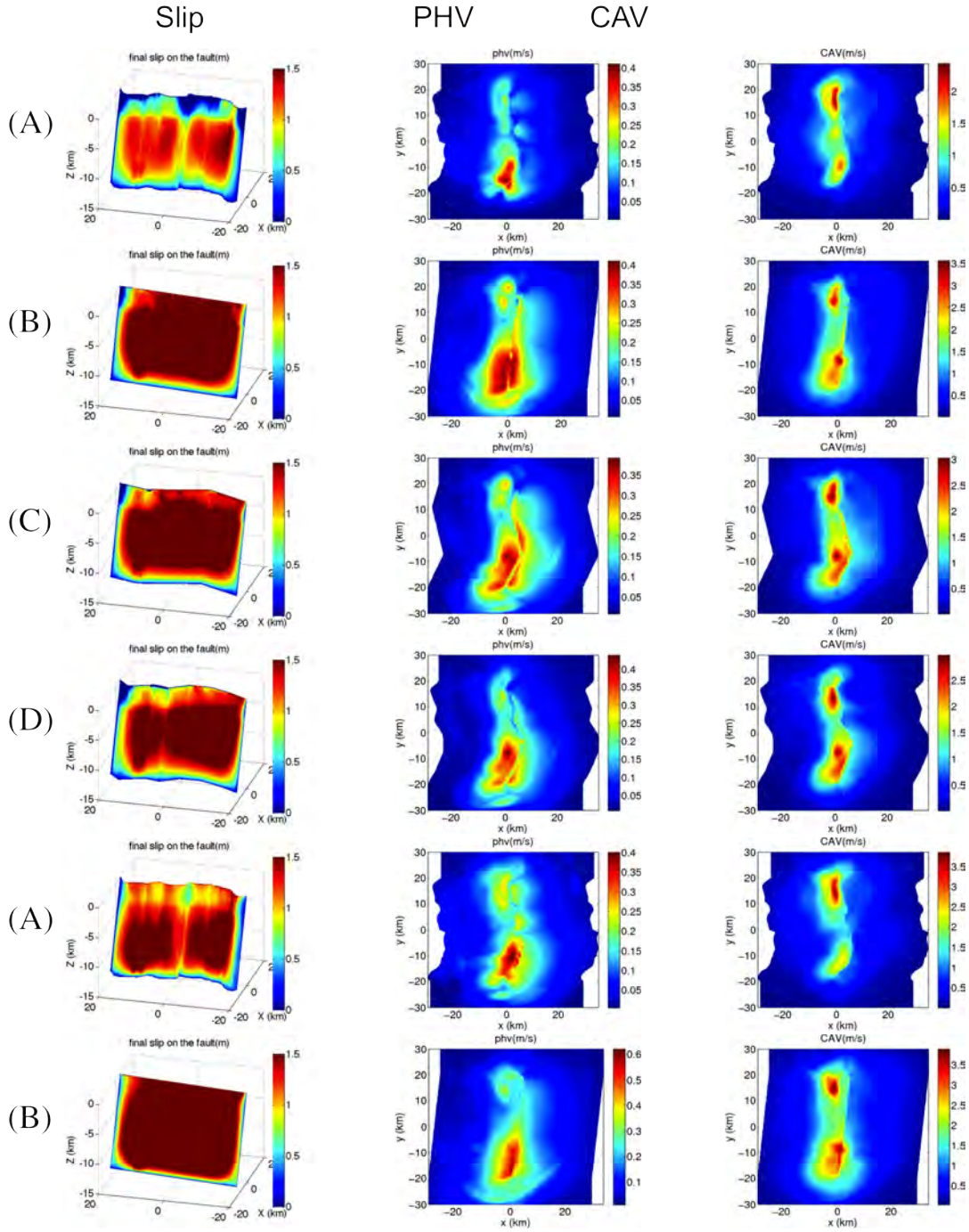

Figure 31: Simulations of fault models A-D with uniform initial stress are the top 4 rows; Bottom 2 rows are simulations for fault models A and B with depth-increasing initial stress. The columns from left to right are final slip distribution on the fault, PHV and CAV distributions in map view.

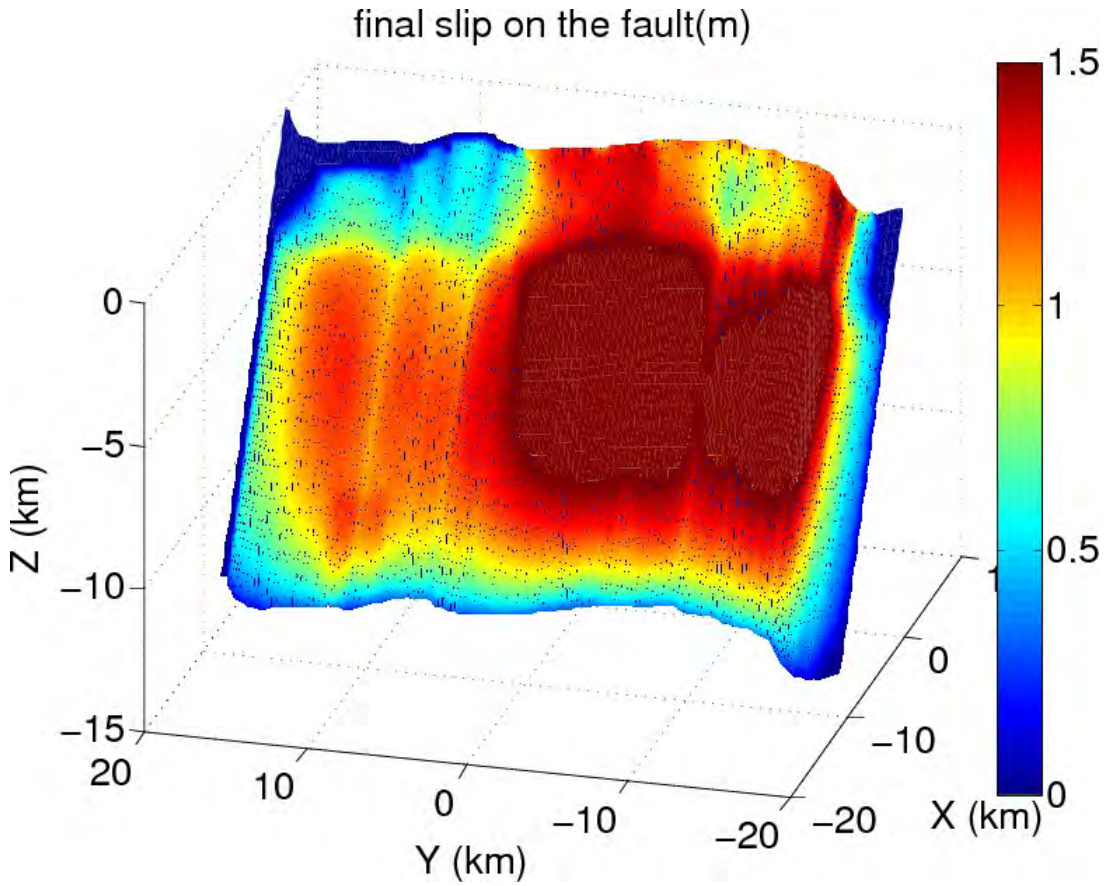

Figure 32: Final Slip on the fault with the smoothed fault model

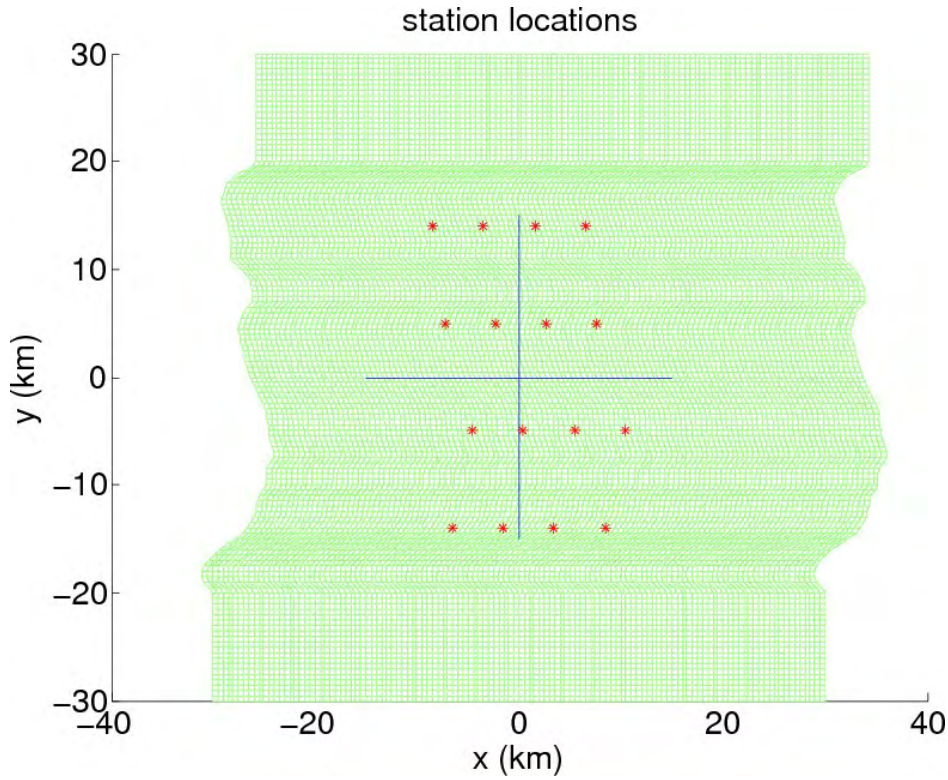

Figure 33: Stations on the surface. X=0 is the approximate location of the strike of the Wasatch Fault.

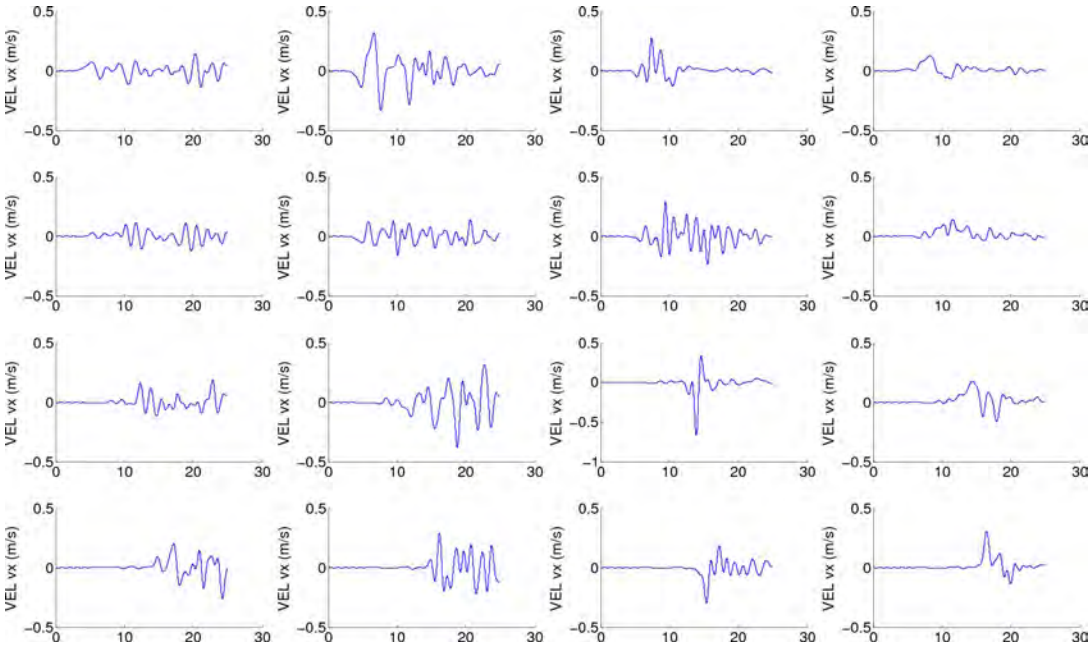

Figure 34: Velocity seismogram at stations (East-West component)

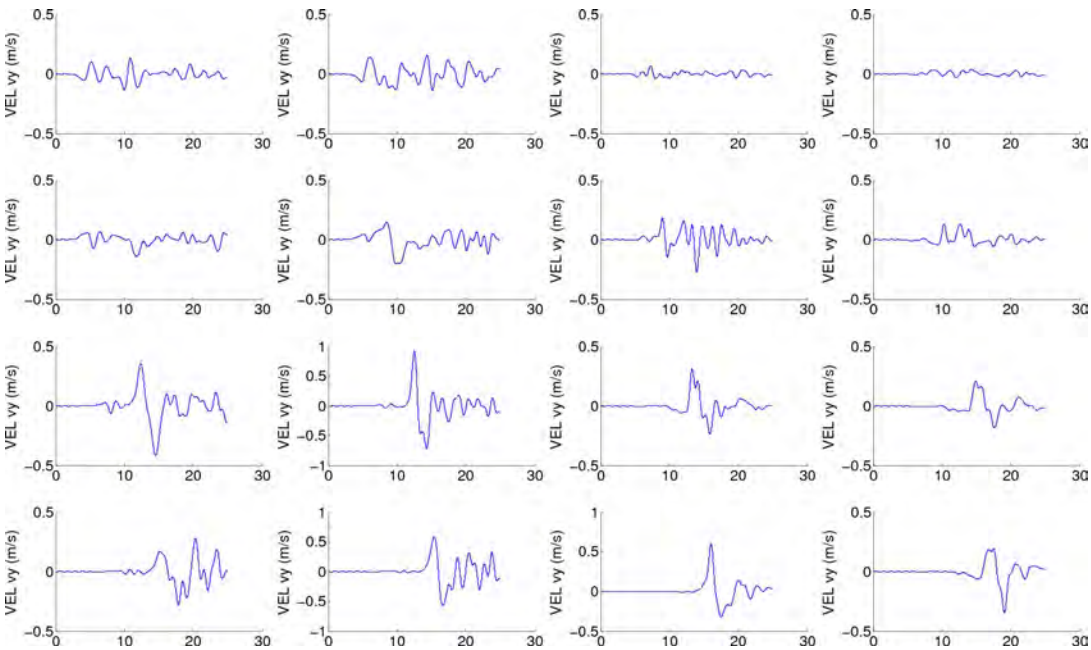

Figure 35: Velocity seismogram at stations (North-South component)

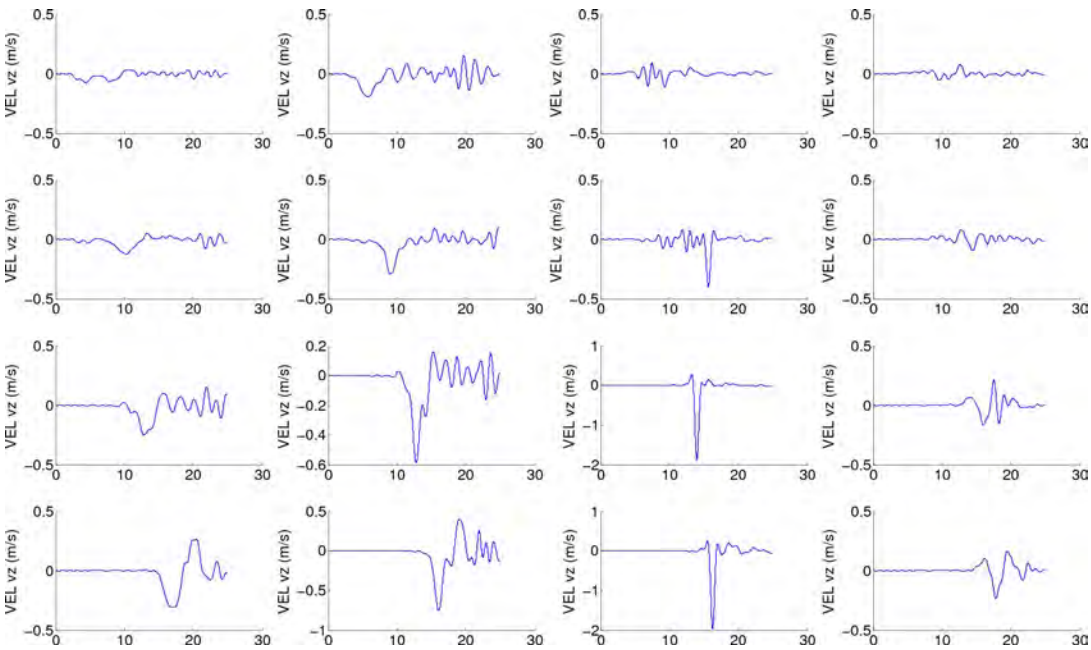

Figure 36: Velocity seismogram at stations (z component)

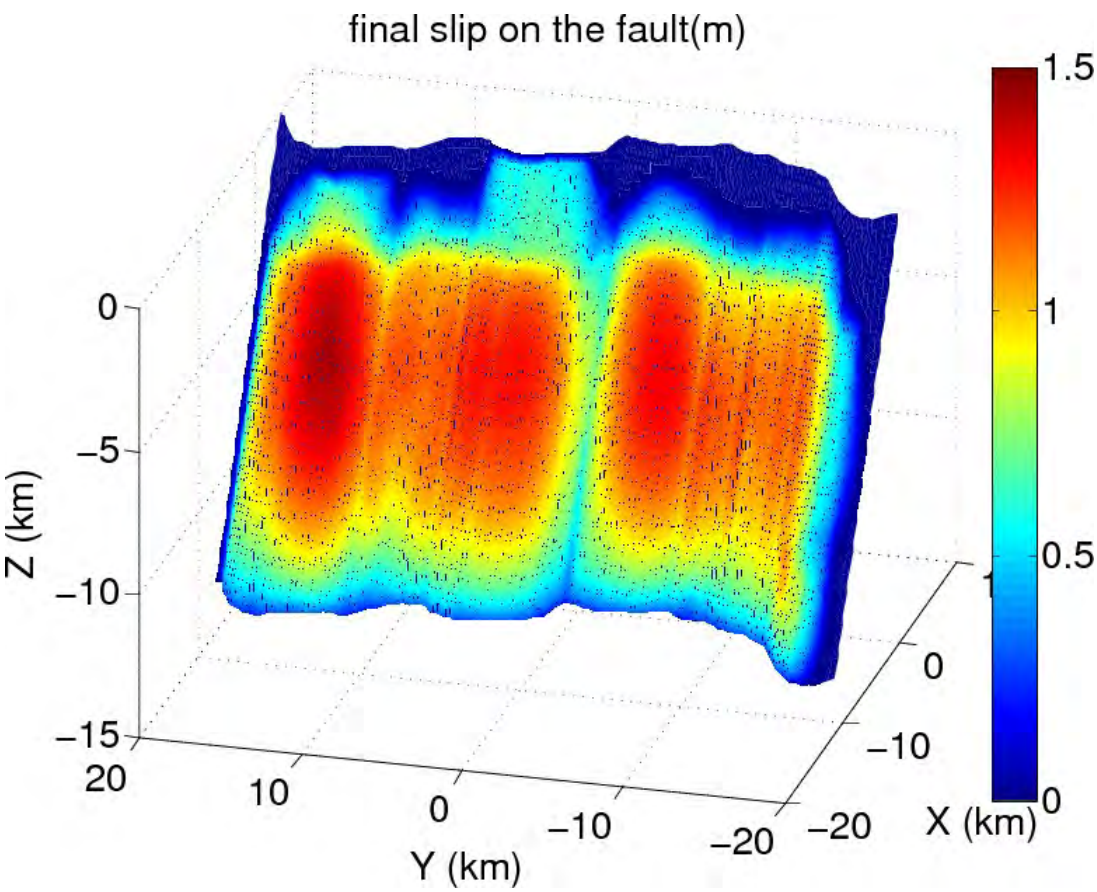

Figure 37: Final slip on the fault with original fault model (with kink)

References:

DuRoss, C. B., Personius, S. F.; Crone, A. J., Olig, S. S., and Lund, W. R. (2011). Integration of paleoseismic data from multiple sites to develop an objective earthquake chronology: Application to the Weber segment of the Wasatch fault zone, Utah, *Bull. Seismol. Soc. Am.* 101, 2765-2781.

Liu, Q. and Archuleta, R.J. (2009). Earthquake Ground Motion for the Salt Lake City Segment of the Wasatch Fault, Eos Trans. AGU, 90(52), Fall Meet. Suppl., Abs S43A-1976.

Liu, Q., Archuleta, R.J., & Smith, R.B. (2010a) Nucleation by Dynamic Triggering on a Multi-Segment Fault, AGU Fall Meeting abstract, *Eos Trans. AGU*, 90, Fall Meet. Suppl., Abs S33E-03.

Liu, Q., Archuleta, R.J., and Smith, R. B. (2010b). Ground Motion from Dynamic Ruptures on the Wasatch Fault Embedded in a 3-D Velocity Structure, *Seismol. Res. Lett.*, 80(2), 320.

Liu, Q., Archuleta, R., & Smith, R. (2011a). Curve Fault Dynamic Rupture Study: Wasatch Fault Salt Lake City Segment, AGU Fall Meeting abstract, *Eos Trans. AGU*, 91(52), Fall Meet. Suppl., Abs S43C-2277.

Liu, Q., Archuleta, R., & Smith, R. (2011b). Does the Tear Fault Matter? (2011 SCEC Annual Meeting poster)

Ma, S. & Liu, P. (2006). Modeling of the perfectly matched layer absorbing boundaries and intrinsic attenuation in explicit finite-element methods. *Bull. Seismol. Soc. Am.* 96, 1779-1794.